



Article

Using Multi-Source Geospatial Information to Reduce the Saturation Problem of DMSP/OLS Nighttime Light Data

Qifei Zhang ^{1,2,3} , Zihao Zheng ^{2,3}, Zhifeng Wu ^{2,4}, Zheng Cao ^{2,*} and Renbo Luo ²

¹ Southern Marine Science and Engineering Guangdong Laboratory, Guangzhou 511458, China; zhangqf@gzhu.edu.cn

² School of Geography and Remote Sensing, Guangzhou University, Guangzhou 510006, China; zhengzh@gzhu.edu.cn (Z.Z.); zfwu@gzhu.edu.cn (Z.W.); luorb@gzhu.edu.cn (R.L.)

³ Department of Land, Environment, Agriculture and Forestry, University of Padova, 35020 Legnaro, Italy

⁴ MNR Key Laboratory for Geo-Environmental Monitoring of Great Bay Area, Shenzhen 518000, China

* Correspondence: jnczdl@gzhu.edu.cn

Abstract: The DMSP/OLS Nighttime light (NTL) data directly reflect the spatial distribution and light intensity of artificial lighting from the Earth's surface at night, and has become an emerging instrument for urbanization research, including in the monitoring of urban expansion, assessment of socio-economic vitality, and estimation of energy consumption and population. However, due to the imperfect sensor design of DMSP/OLS, the dynamic range of the digital number (DN) of NTL is limited (0, 63), leading to a significant saturation problem when describing the actual light intensity, especially in dense urban areas with high light intensity. This saturation problem masks spatial differences in light intensity and weakens the reliability of DMSP/OLS NTL data. Therefore, this study proposes a novel desaturation indicator that combines NDBI and POI, the Building and POI Density-Adjusted Nighttime Light Index (BPANTLI), to regulate the DMSP/OLS NTL saturation problem based on the spatial characteristics of urban structures and human activity intensity. The proposed method is applied to three urban agglomerations with the most severe light saturation issues in China. The geographical detector model is firstly utilized to quantify the effectiveness of NDBI and POI in reflecting the difference in light intensity distribution from the NTL potential saturation region (NTL DN value (53, 63)) and NTL unsaturation region (NTL DN value (0, 52)), so as to clarify the feasibility of developing the BPANTLI. The applicability of BPANTLI is validated through three aspects—comparison of the desaturation capacity and the performance of delineating light intensity; verification of the consistency of BPANTLI with radiometric calibration nighttime light product (RCNTL) and NPP/VIIRS data; and assessing the accuracy of the BPANTLI in estimating socio-economic parameters (GDP, electricity consumption, population density). The results indicate that the BPANTLI possesses superior capability in regulating the NTL saturation problem, achieving good performance in distinguishing inner-urban structures. The regulated results reveal a remarkably improved correspondence with the RCNTL and NPP/VIIRS data, providing a more realistic picture of the light intensity distribution. It is worth noting that, given the advantages of NDBI and POI vector data in spatial resolution, the BPANTLI established in this study can overcome the limitation of the spatial resolution of DMSP/OLS nighttime lighting data and achieve dynamic transformation of the spatial resolution. The higher spatial resolution desaturation results allow for a better characterization of the light intensity distribution. Moreover, the BPANTLI-regulated light intensity significantly improves the accuracy of estimating electricity consumption, GDP, and population density, which provides a valuable reference for urban socio-economic activity assessment. Thus, the BPANTLI proposed in this study can be considered as a reasonable desaturation method with a high application value.

Keywords: Defense Meteorological Satellite Program/Operational Line-Scan System (DMSP/OLS); nighttime light data (NTL); saturation problem; NDBI; POI



Citation: Zhang, Q.; Zheng, Z.; Wu, Z.; Cao, Z.; Luo, R. Using Multi-Source Geospatial Information to Reduce the Saturation Problem of DMSP/OLS Nighttime Light Data. *Remote Sens.* **2022**, *14*, 3264. <https://doi.org/10.3390/rs14143264>

Academic Editors: Bailang Yu and Johannes Puschig

Received: 25 May 2022

Accepted: 4 July 2022

Published: 6 July 2022

Publisher's Note: MDPI stays neutral with regard to jurisdictional claims in published maps and institutional affiliations.



Copyright: © 2022 by the authors. Licensee MDPI, Basel, Switzerland. This article is an open access article distributed under the terms and conditions of the Creative Commons Attribution (CC BY) license (<https://creativecommons.org/licenses/by/4.0/>).

1. Introduction

In recent decades, the rapid expansion of urban agglomerations has become a pervasive spatial phenomenon in global urbanization. The Defense Meteorological Satellite Program/Operational Linescan System (DMSP/OLS) can detect visible light at night, which can intuitively reflect the structural details and spatial distribution of metropolitan areas, urban traffic corridors, and even intensity of human activity [1–5]. This Nighttime light (NTL) data records the spatial distribution and light intensity of artificial lighting from the Earth's surface at night, and has been widely and effectively used in urbanization research, including urbanization level assessment [6,7], monitoring of urban expansion [8,9], and estimating energy consumption [10–12], gross domestic product [13–15], and population [16,17].

Although the new generation of NPP/VIIRS DNB data has better performance in spatial resolution and radiation calibration of the NTL [18–21], the DMSP/OLS NTL dataset has become the most widely used and irreplaceable NTL product due to its long-term historical monitoring. However, due to the imperfect sensor design of DMSP/OLS, the dynamic range of the NTL digital number (DN) is limited to 0–63. This low dynamic range leads to the saturation problem of NTL data when describing the actual surface light intensity, especially in dense urban areas with strong light intensity. That is, the DN value increases to a certain extent and no longer continues to increase with the increase of light intensity, which limits the range of brightness measurement. This means that the light intensity expressed by the DN value is much lower than the actual value, especially in urban areas where the light intensity is relatively high [22–24]. Such saturation problems not only lead to the underestimation of the actual light intensity, but also limit the description of inner-urban variations in light intensity. This defect undoubtedly reduces the application accuracy of NTL data. Therefore, effectively overcoming the saturation problem of DMSP/OLS NTL data has become one of the current research foci.

At present, the approach to alleviating the DMSP/OLS NTL data saturation problem can be summarized into three aspects: statistical extrapolation method, radiometric calibration method, and indicator-based correction method [25–29]. The first method is mainly based on time series NTL data for cross-calibration or assumes a consistent spatial trend or histogram distribution of DN value in the saturated and unsaturated regions. For example, Cao et al. [30] used invariant target regions to perform mutual correction on DMSP/OLS NTL data. Letu et al. [31] developed a cubic regression method to correct the saturation problem based on the spatial distribution pattern of stable light. Although this method is theoretically sound and has high accuracy, the OLS sensor is not equipped with an onboard calibration system (low gain equipment) for the radiometric calibration method. Therefore, it is difficult to calibrate the NTL data using the radiation calibration method. Currently, only the National Geophysical Data Center (NGDC) has released some time-specific radiometric calibration NTL products (RCNTL). In view of this, Letu et al. [32] constructed a linear regression between the 1996–1997 radiation calibration NTL products and the non-saturated part of 1999 NTL data; thus, calculating the light intensity in the saturation region of the 1999 NTL data. However, this method assumes that the actual DN value of saturated pixels hardly changed during 1996–1999. This assumption may be applicable in highly developed countries, but it is difficult to guarantee for regions with rapid urbanization progress (such as in China). As for the indicator-based correction method, prior efforts have developed vegetation-based correction indicators (HSI, VANUI, EANTLI, LERNCI) based on the negative correlation between vegetation abundance and human activities [33–37]. These methods assume that places with low vegetation coverage, such as urban centers, typically have stronger socio-economic vitality and therefore have a greater NTL intensity. Specifically, vegetation indices (NDVI, EVI) are employed to develop vegetation-based correction indicators and subsequently utilized to establish a relationship with light intensity, so as to correct the saturation problem. For example, Lu et al. [33] and Zhang et al. [34] both utilized the NDVI to develop the Human Settlement Index (HSI) and Vegetation Adjusted NTL Urban Index (VANUI) to regulate the saturation problem, and the results showed that the light intensity in the saturated area of the city was well corrected.

Compared with the NDVI, the Enhanced Vegetation Index (EVI) has the advantage of overcoming the NDVI saturation and attenuating the influence of soil background and atmosphere on the NDVI. Therefore, Zhuo et al. [35] proposed the Enhanced Vegetation Index-Adjusted Nighttime Light Index (EANTLI) based on the EVI to alleviate the saturation problem. Their results indicate that the EANTLI is capable of reducing NTL saturation and significantly increases spatial heterogeneity in saturated areas, effectively alleviating the NTL saturation problem. In order to break through the insufficiency of a single index (NDVI, EVI) to construct desaturation indicators, Liu et al. [37] introduce the land surface temperature (LST) on the basis of the vegetation index to construct the LST- and EVI-regulated NTL city index (LERNCI), which achieves good performance in reducing and regulating the NTL saturation phenomenon. In addition to vegetation-based indicators, Zheng et al. [38] utilized social sensing data to develop the Vector-Data-Adjusted NTL Index (VDANTLI) to alleviate the saturation phenomenon. Although this method achieves a satisfactory correction effect, the social sensing data is usually sporadically distributed in urban suburbs, which poses a challenge to global correction.

In fact, for the indicator-based correction method, the correction effect of the NTL saturation problem is inextricably linked to the correction indicators. It is well recognized that light intensity is closely related to urbanization level and socio-economic activity. For example, light intensity in urban central business districts with high socio-economic activity intensity is undoubtedly much greater than in suburbs and rural areas. However, it is found that most of the current correction indicators are developed based on vegetation indices (NDVI, EVI). Although in most situations, these vegetation-based indicators alleviate the saturation problem of NTL data, the reasonableness of the assumption of negative correlation between vegetation coverage and human activities remains somewhat problematic, especially for cities where urbanization is less consistent with the distribution of green spaces. Firstly, vegetation abundance is only a tangential reflection of the urbanization level, and cannot fully reflect regional social and economic vitality. For example, the vegetation coverage of water bodies or bare land is relatively low, but this does not mean that the socio-economic activity or urbanization rate is high in these areas. In fact, the light intensity of rivers and lakes is much less intense than in urban centers. Therefore, this may lead to an overestimation of the light intensity in water bodies and bare land. Moreover, the EVI values for water bodies are close to zero, resulting in abnormally high EANTLI values, which leads to an inconsistency with reality. Secondly, with the continuous improvement of the quality of human settlements, the vegetation coverage of urban centers is gradually increasing. This implies that the urbanization rate may not be consistent with the vegetation distribution. Therefore, we cannot simply assume that where the vegetation cover is high, the light intensity is necessarily low. Thirdly, the difference in vegetation coverage in central urban areas is not obvious, especially for rapidly urbanizing cities. Although fine-scale urban green space cover products are currently available [39], most of the previous efforts only utilized NDVI or EVI derived from MOD13A3 products. Using vegetation coverage with low spatial heterogeneity to regulate the saturation problem may not have the capability to delineate the spatial distribution of NTL. Additionally, for cities with rapid urbanization, the difference in vegetation coverage in central urban areas is not obvious. All these interference factors make it difficult to achieve satisfactory performance in regulating NTL saturation images.

Considering the above deficiencies, this article aims to develop a more robust and effective desaturation indicator to adequately address the NTL saturation problem. Given the NTL is highly consistent with human activity, we attempted to propose a novel correction indicator to regulate the light saturation problem from the perspectives of urban built-up areas and intensity of socio-economic activity. Firstly, the Normalized Difference Built-up Index (NDBI) is a remote sensing index that can quickly and accurately extract urban built-up areas and has been widely used in urban studies [40–45]. Additionally, the NDBI value is positively correlated with light intensity, avoiding outliers caused by low vegetation index value in water bodies and bare land. Secondly, this study further

adopts the point of interest (POI), a new location-based service data type, to characterize the intensity of socio-economic activity. POI refers to point data that record the spatial location and attribute information of geographical entities, such as shopping malls, restaurants, shops, supermarkets, schools, hospitals, parks, and government agencies [46–48]. The spatial distribution pattern and density of POI can intuitively reflect the distribution of various urban facilities and the characteristics of social behavior. Theoretically, regions with more active socio-economic intensity also have higher POI density. For example, the POI density in city centers (CBD) will be much greater than that in suburban or rural areas. Additionally, in some extreme cases, such as abandoned towns, where the NTL intensity is very low (without human activity) despite the high proportion of urban built-up areas, POI density can effectively avoid this overestimation error.

Based on the abovementioned idea, this study introduces a novel desaturation indicator that combines NDBI and POI, namely the Building and POI Density-Adjusted Nighttime Light Index (BPANTLI), to regulate the NTL saturation problem and delineate spatial differences in light intensity more robustly and effectively. Moreover, to verify the performance of the BPANTLI, we compared it with other correction indicators (HSI, VANUI, EANTLI), radiometric calibration NTL, NPP/VIIRS data, and evaluated the accuracy of estimating socio-economic factors (electricity consumption, GDP, population density). Three major urban agglomerations in China with the most severe light saturation problems are selected as the test areas for validation of the proposed indicator.

2. Materials and Methods

2.1. Study Area

In this study, three major urban agglomerations: Beijing–Tianjin–Hebei (BTH), Yangtze River Delta (YZD), and Pearl River Delta (PRD) urban agglomerations are selected as study areas (Figure 1). The three urban agglomerations are located in North China (BTH), East China (YZD), and South China (PRD), all of which are important political, economic, cultural, and scientific centers for China. They are located between $112^{\circ}45'E$ and $123^{\circ}25'E$ and between $21^{\circ}31'N$ and $42^{\circ}40'N$, with an area of 218,000 km², 211,000 km², and 42,200 km², respectively. Since the reform and open-up policy, these urban agglomerations have experienced dramatic urbanization, and have become the most developed and economically dynamic regions in China. The GDP of BTH, YZD, and PRD urban agglomerations in 2019 has reached \$1.3 trillion, \$3.6 trillion, and \$1.8 trillion, respectively, accounting for 44% of the total GDP of China. Meanwhile, at the end of 2020, the resident population of these three metropolitan regions reached 112 million (BTH), 235 million (YZD), and 64 million (PRD) respectively, accounting for 29.2% of the population of mainland China. The vibrant socio-economic activity has increased the light intensity in these three urban agglomerations, leading to severe saturation problems. Therefore, examining the proposed BPANTLI in these three urban agglomerations possesses a certain representativeness and significance.

Considering the data collection, Beijing, Tianjin, Tangshan, and Langfang cities were selected for BTH urban agglomeration; Shanghai, Nanjing, Hangzhou, Changzhou, Ningbo, Wuxi, Suzhou, Huzhou, Shaoxing, Jiaxing, and Nantong cities were selected for the YZD urban agglomeration; Guangzhou, Shenzhen, Foshan, Dongguan, Zhuhai, Huizhou, Zhongshan, Jiangmen, and Zhaoqing cities are selected for the PRD urban agglomeration; coming to a total of 24 cities. Table 1 provides a summary of the socio-economic conditions for those 24 cities.

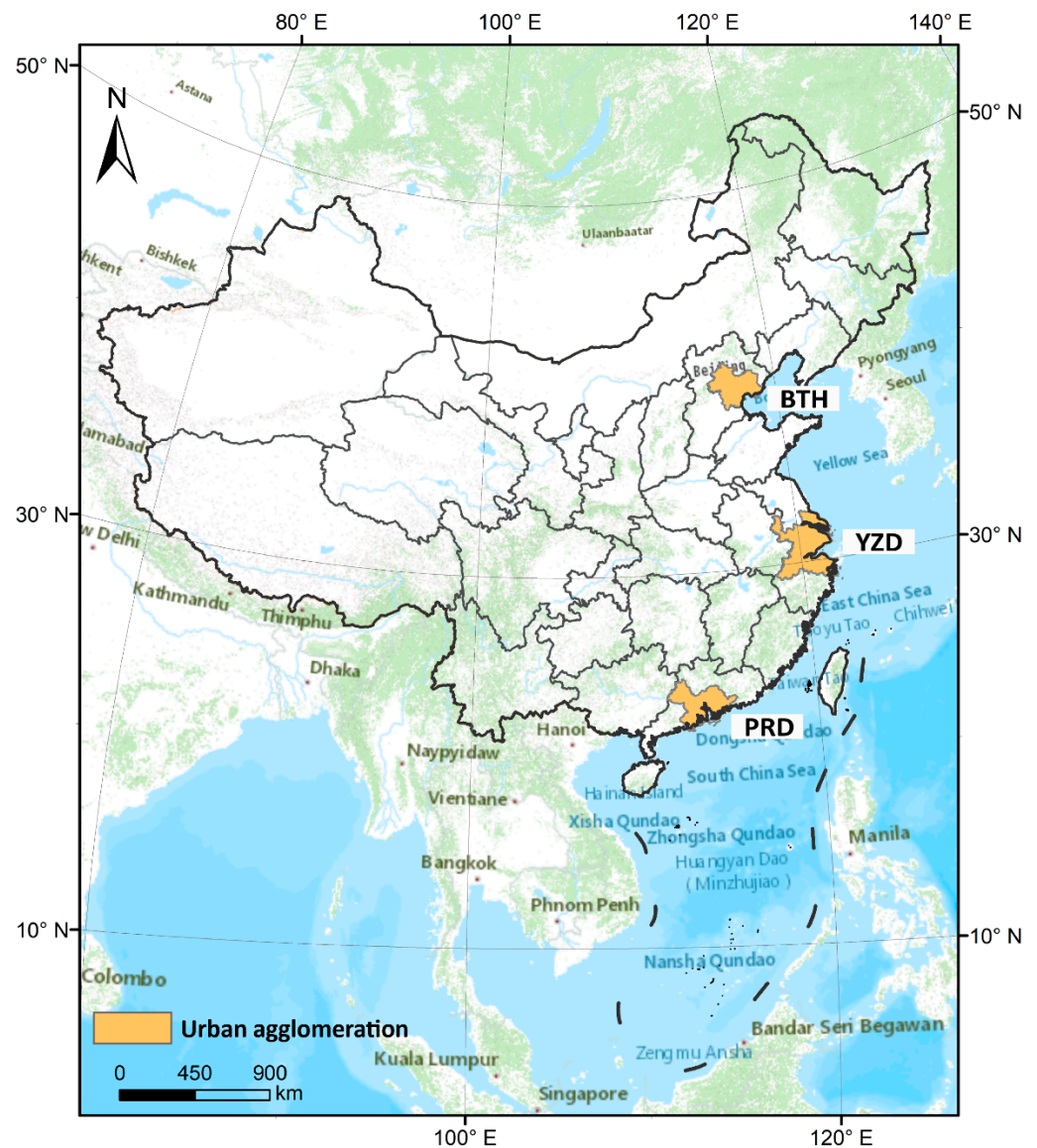


Figure 1. The location of the three major urban agglomerations in China.

Table 1. Overview of the administrative areas, population, and gross domestic product (GDP) of the selected 24 prefecture-level cities.

City	Administrative Areas (km ²)	Population (Million)	Electricity Consumption (Billion kwh)	GDP (Billion RMB)
Beijing	15,863.29	13.16	91.31	1950.06
Tianjin	11,916.85	14.72	82.34	1437.02
Tangshan	13,471.92	7.47	75.73	612.12
Langfang	6429.31	5.46	13.09	194.31
Shanghai	6340.50	24.15	141.06	2160.21
Nanjing	6587.02	6.43	46.27	801.17
Hangzhou	16,596.75	8.84	63.85	834.35
Changzhou	4372.15	4.69	39.10	436.09

Table 1. Cont.

City	Administrative Areas (km ²)	Population (Million)	Electricity Consumption (Billion kwh)	GDP (Billion RMB)
Ningbo	9816.28	5.80	55.94	712.88
Wuxi	4627.46	4.72	60.64	807.02
Suzhou	8488.42	6.53	126.32	1301.57
Huzhou	5819.85	2.62	18.29	180.31
Shaoxing	8279.02	4.94	35.96	396.73
Jiaxing	3915.34	3.46	38.55	314.76
Nantong	8001.11	7.66	60.05	503.88
Guangzhou	7434.40	8.32	71.07	1542.01
Shenzhen	1996.78	10.62	72.98	1450.02
Foshan	3797.72	7.29	57.76	701.07
Dongguan	2459.85	8.31	62.25	549.02
Zhuhai	1724.32	1.59	12.17	166.23
Huizhou	11,343.12	3.43	24.84	267.83
Zhongshan	1800.14	3.17	21.71	263.89
Jiangmen	9505.42	3.93	20.73	200.02
Zhaoqing	14,891.22	4.29	10.78	166.01

2.2. Data

In this study, the data contain F18 DMSP/OLS stable NTL data (version 4, 1992–2013), radiometric calibration nighttime light product (RCNTL), Landsat TM/ETM data, POI data, MODIS MOD13A3 annual average monthly vegetation index data products (NDVI, EVI), GPWv4 global population density data (PD), Gross Domestic Product (GDP), and annual electricity consumption (EC) of the study area (Table 2). We take 2013 as the time node, the average visible and cloud-free DMSP/OLS stable NTL products were selected as the correction object. The RCNTL and National Polar-orbiting Partnership/Visible Infrared Imaging Radiometer Suite (NPP/VIIRS) data were adopted to examine the performance of the saturation effect correction. The cloud-free Landsat TM images covering these three urban agglomerations were selected to calculate the NDBI. The POI data was obtained from the AutoNavi map. Due to the huge amount of POI data, four types of POI data that are closely related to socio-economic activity are selected for this study (commercial locations, dining locations, entertainment locations, and residential locations). The vegetation indices (NDVI, EVI) were derived using the MOD13A3 product to construct vegetation-based desaturation indicators. The GPWv4 population density data (PD) was provided by NASA's Earth-Observing System Data and Information System (EOSDIS). Since this data is updated every 5 years, the global population density data in 2015 was selected as the data source for this paper. The GDP and electricity consumption (EC) of each prefecture-level city in three urban agglomerations were calculated from the statistical yearbook. All data were reprojected to the WGS-84 coordinate system.

Table 2. Overview of data used in this study.

Data	Resolution	Time	Data Source
DMSP/OLS nighttime light (NTL)	30 arc second	2013	NOAA/NGDC (http://ngdc.noaa.gov/eog/download.html) accessed on 1 May 2022
Radiometric calibration nighttime light (RCNTL)	30 arc second	2013	

Table 2. Cont.

Data	Resolution	Time	Data Source
National Polar-orbiting Partnership/Visible Infrared Imaging Radiometer Suite (NPP/VIIRS)	15 arc second	2013	Earth Observations Group (https://www.ngdc.noaa.gov/eog/viirs/download_dnb_composites.html) accessed on 1 May 2022
Landsat TM/ETM	30 m	2013	USGS (https://earthexplorer.usgs.gov/) accessed on 1 May 2022
POI	Point data	2013	OpenStreetMap (http://download.geofabrik.de/) accessed on 1 May 2022
MODIS MOD13A3	1 km	2013	MODIS (https://modis.gsfc.nasa.gov/) accessed on 1 May 2022
GPWv4 population density (PD)	1 km	2015	EOSDIS (http://sedac.ciesin.columbia.edu/data/collection/gpw-v4) accessed on 1 May 2022
Gross Domestic Product (GDP)	-	2013	China Statistical Yearbooks Database (http://www.shujuku.org/)
Annual electricity consumption (EC)	-	2013	accessed on 1 May 2022

2.3. Methods

In this study, we propose a novel socio-economic-activity-based desaturation indicator BPANTLI to regulate the NTL saturation problem more robustly and effectively. This approach can be divided into three main steps (Figure 2). Firstly, multi-source data with different spatial resolutions are unified into 500 m areas through grid processing and normalization. Secondly, the geographical detector model was utilized to quantify the effectiveness of NDVI, EVI, NDBI, and POI in reflecting the difference in light intensity distribution from two levels: the NTL potential saturation region (NTL DN value (53, 63)) and NTL unsaturation region (NTL DN value (0, 52)), thereby verifying the feasibility of mitigating the saturation problem based on the combination of NDBI and POI. Further, the BPANTLI desaturation indicator was developed based on the explanatory power of the interactive detectors from the geographical detector model. Lastly, the applicability of BPANTLI is evaluated through (1) the verification of the desaturation capacity and the performance of delineating light intensity; (2) the consistency of BPANTLI with RCNTL and NPP/VIIRS data; (3) the corresponding correlation between BPANTLI and socio-economic parameters (electricity consumption, GDP, and population density) from the prefecture level and pixel level.

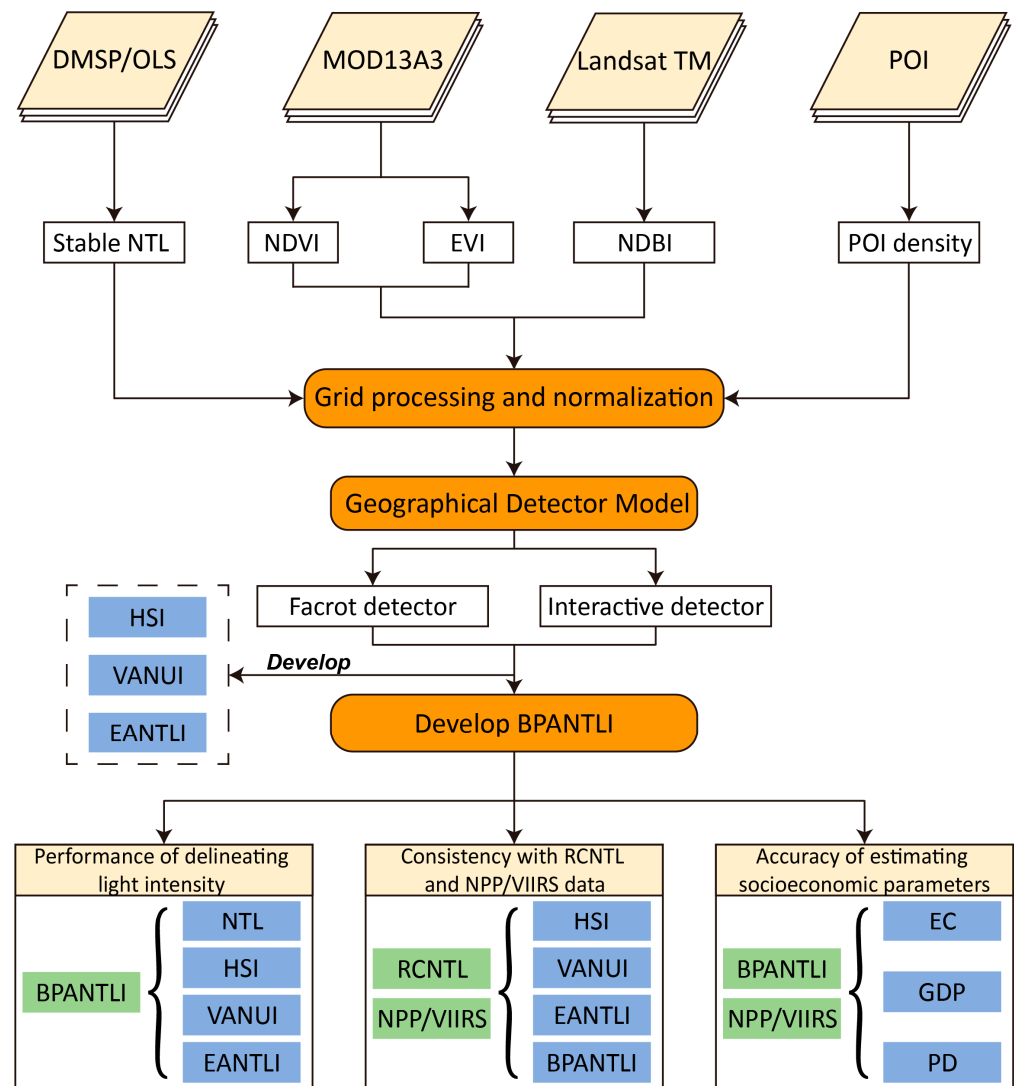


Figure 2. The integrated framework of the methodology employed in this study.

2.3.1. Data Normalization and Grid Processing

Firstly, as each data has a different value domain, this study further normalizes the attribute data within each grid unit (0, 1) to facilitate calculation and analysis. Additionally, considering the different spatial resolutions of each data source, the create fishnet tool in ArcGIS Pro was adopted to construct a fishnet with a resolution of 500 m. Then the zonal statistics tool was utilized to extract the NTL DN values, NDVI, EVI, NDBI, and POI information for each grid unit, so as to realize the unification of multi-source data. That is to say, the attribute information (light intensity, vegetation index, NDBI, POI) from the multi-source dataset is unified to a grid unit with a resolution of 500 m. Based on this, these grid units containing attribute information and consistent spatial resolution lay a foundation for subsequent quantitative and qualitative analysis.

2.3.2. Geographical Detector Model

The geographical detector model is the new spatial statistical analysis model that can effectively diagnose the spatial heterogeneity of landscape elements [49–51]. The principle of this model is based on stratified spatial heterogeneity, which can either examine the spatial heterogeneity of a single variable or detect the interaction of two factors on a dependent variable. This method has no linear hypothesis, which effectively overcomes the

limitations of the traditional statistical methods which have been widely used to explain the degree of spatial distribution differences in geographical phenomena [39,52,53].

According to the characteristics of NTL data, this study measures the spatial correlation of NDVI, EVI, NDBI, and POI with NTL distribution from two levels of light potential saturation region and light unsaturation region. Given that the RCNTL offers a perfect correlation with nighttime light data from DMSP-OLS, this study introduces the RCNTL into the geographical detector model as a baseline for verifying the effectiveness of NDVI, EVI, NDBI, and POI data in reflecting the differences in the spatial distribution of NTL in saturated and unsaturated regions. The factor detector of the geographical detector model uses the *q* value to measure the degree of explanation of NDVI, EVI, NDBI, and POI on the spatial distribution difference of NTL. The *q* value is between 0 and 1, a higher *q* value indicates that the NDVI, EVI, NDBI, or POI can better reflect the distribution of NTL. When the *q* value is 0, it means that there is no relationship between NDVI, EVI, NDBI, or POI and NTL. In addition, in order to judge whether the combination of different indexes (NDVI, EVI, NDBI, POI) can more fully reflect the distribution pattern of NTL, this study further uses the interactive detector to quantify the interaction effect of two separate indexes on NTL distribution. The interactive detector calculates and compares the *q* value of each single factor and the *q* value of the superposition of the two factors, and then judges whether there is an interaction between the two factors and the strength, direction, linearity, or nonlinearity of the interaction.

2.3.3. Developing BPANTLI

It is known that light intensity is inextricably linked to human activity, with both NDBI and POI showing positive trends in relation to human activity intensity. Therefore, in this study, we combine NDBI and POI to develop the BPANTLI based on the results of the interactive detectors of the geographical detector model. The process of constructing the BPANTLI desaturation indicator is shown in Figure 3.

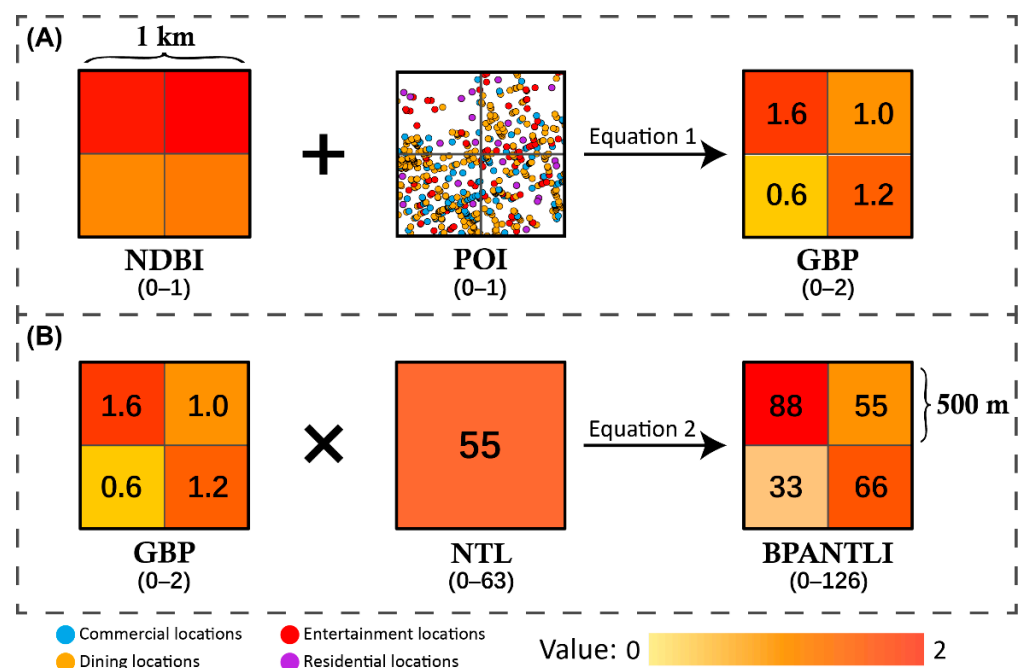


Figure 3. The process of regulating the saturation problem through the BPANTLI. (A) Summing the NDBI value and POI density; (B) Multiplying GBP value with original NTL data.

Given the high proportion of impervious surfaces and the intensity of socio-economic activities in cities, both NDBI value and POI density are higher in urban centers. In rural areas, however, the values of NDBI and POI density tend to be relatively low. Meanwhile,

the light intensity in urban areas tends to be more intense than in suburban areas. This indicates that the light intensity has a good consistency with NDBI value and POI density, all decreasing from the urban center to the suburbs. Notably, the value of NDBI and POI density are both normalized, which means that the maximum value of these two parameters is 1. Therefore, we further sum the NDBI value and POI density (using GBP to represent) to enhance the difference in human activity intensity (Figure 3A). This means that the closer to the city center, the larger the value of the NDBI and POI, and the correspondingly larger the GBP value, with a maximum value of 2 (both NDBI and POI values are 1). Conversely, the further away from the city center, the smaller the value of the NDBI and POI value, and thus the smaller the GBP value, with a minimum value of 0 (both NDBI and POI values are 0). This suggests that greater GBP values are more likely (often greater than 1) in areas with potential NTL saturation, such as central business districts. On the contrary, in areas where NTL data generally does not have saturation problems (e.g., suburbs), the GBP value is likely to be smaller (often less than 1). Based on this variation characteristic, we consider the GBP value as an adjustment coefficient and multiply it with the original NTL data (Figure 3B). In other words, the regional light intensity can be increased or decreased depending on the value of the GBP. The BPANTLI calculated on the basis of NDBI and POI further increases the difference between urban centers and suburbs, thus expanding the spatial differences in NTL intensity between the saturation region and unsaturation region.

$$\text{GBP} = \text{NDBI}_{\text{norm}} + \text{POI}_{\text{norm}} \quad (1)$$

$$\text{BPANTLI} = \text{GBP} \times \text{NTL} \quad (2)$$

It is worth noting that this study regulates the saturation problem based on the NDBI value and POI density in the grid units, which means that the spatial resolution of BPANTLI is determined by the size of the grid units. For example, the spatial resolution of the fishnet is set to 500 m in this study (Figure 3). As a result, the spatial resolution of the regulated light intensity (BPANTLI) is improved from 1 km to 500 m, which breaks through the inherent spatial resolution of DMSP/OLS NTL data (Figure 4). The BPANTLI with higher spatial resolution may have better performance in urban studies (urbanization level assessment, energy consumption estimation). Moreover, multiple resolution grid units can be created according to research needs to realize the dynamic transformation of the BPANTLI spatial resolution, thereby overcoming the limitation of DMSP/OLS NTL data spatial resolution.

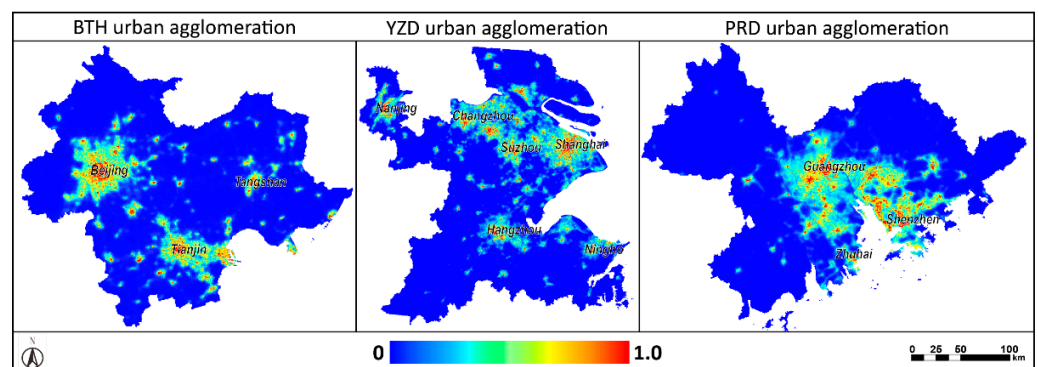


Figure 4. The BPANTLI in three major urban agglomerations (Beijing–Tianjin–Tangshan Region, Yangtze River Delta, and Pearl River Delta) in China.

2.3.4. BPANTLI Validation

(1) Comparison between HSI, VANUI, EANTLI, and BPANTLI

In this study, HSI, VANUI, and EANTLI desaturation indicators were also calculated to compare the desaturation effect and the differentiation of light intensity in the NTL saturation region with BPANTLI. Among them, the HSI, VANUI, and EANTLI are calculated

according to the method proposed by Lu et al. [33], Zhang et al. [34], and Zhuo et al. [35], and the calculation formulas are as follows:

$$\text{HSI} = \frac{(1 - \text{NDVI}) + \text{NTL}}{(1 - \text{NTL}) + \text{NDVI} + \text{NDVI} \times \text{NTL}} \quad (3)$$

$$\text{VANUI} = (1 - \text{NDVI}) \times \text{NTL} \quad (4)$$

$$\text{EANTLI} = \frac{1 + (n\text{NTL} - \text{EVI})}{1 - (n\text{NTL} - \text{EVI})} \times \text{NTL} \quad (5)$$

The NDVI and EVI data used to calculate HSI, VANUI, and EANTLI are from the MODIS MOD13A3 product. In order to carry out consistent comparisons, all calculation results are normalized to a range of (0, 1). In order to assess the ability of BPANTLI to regulate the saturation problem, this study further selects typical NTL saturation regions in BTH, YZD, and PRD urban agglomeration to compare the capability of each indicator to regulate the NTL saturation problem and the distinguishability of light intensity (Figure 5).

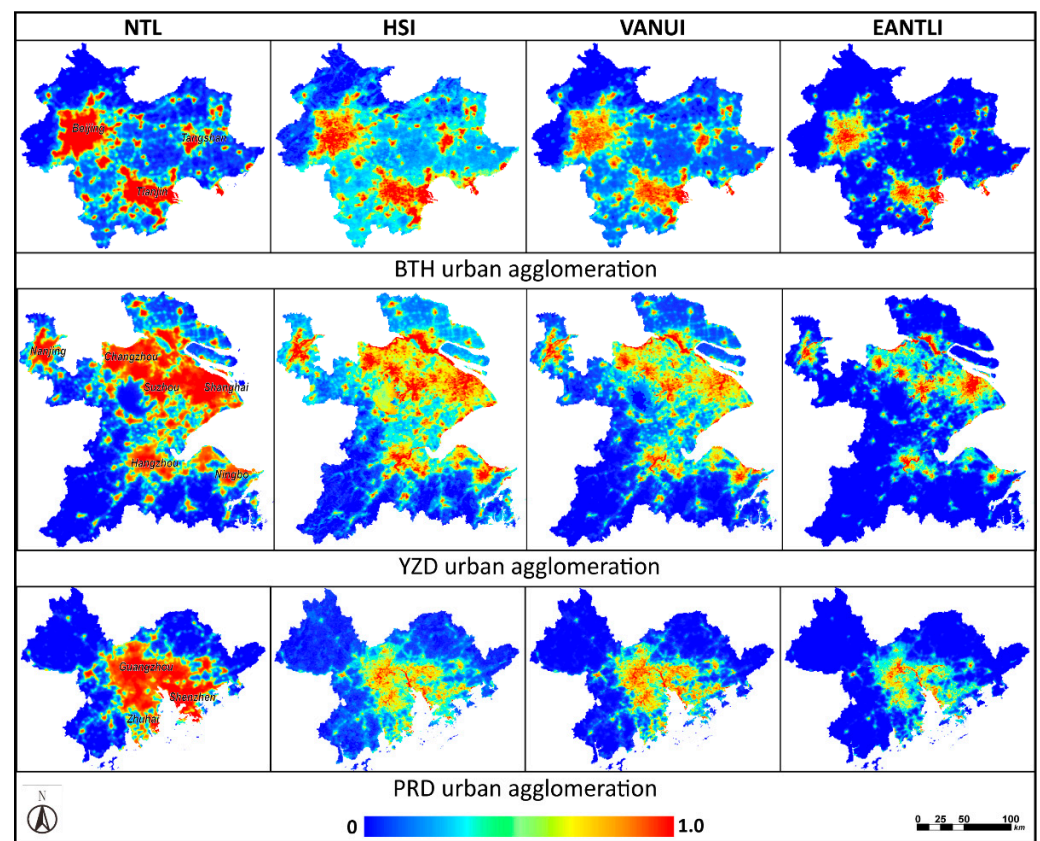


Figure 5. The normalized NTL data and three desaturation indicators (HSI, VANUI, EANTLI) in three urban agglomerations.

(2) Similarity with RCNTL and NPP/VIIRS data

Considering the accuracy and absence of a pixel saturation problem of RCNTL and NPP/VIIRS data, this study selected these data as a criterion for comparative verification. Firstly, three transects through the BTH, YZD, and PRD urban agglomeration saturation regions are selected to compare the differences between NTL, BPANTLI, and RCNTL. Secondly, the regression analysis was performed on HSI, VANUI, EANTLI, BPANTLI, and RCNTL, NPP/VIIRS data on the transects. The correlation coefficients were then calculated and compared to validate the correspondence between BPANTLI and RCNTL, and NPP/VIIRS data, so as to verify the desaturation ability of BPANTLI.

(3) Capacity to estimate electricity consumption, GDP, and population density

In recent years, since light intensity can mirror the spatial distribution of human activities, many scholars have conducted studies on estimating socio-economic indicators such as population density, GDP, and energy consumption using NTL data [25,32,54–56]. Therefore, in this paper, the electricity consumption, GDP, and population density at the prefecture level were selected for regression analysis with NTL, VANUI, EANTLI, BPANTLI, and NPP/VIIRS, respectively, so as to evaluate the respective correlation among them. Additionally, this study further generates 500 random sampling points within the potential saturation region and NTL unsaturation region in different level cities (Beijing, Shanghai, Guangzhou, Shenzhen, Foshan) to examine the adequacy of fit between BPANTLI and population density at the pixel level. Considering the spatial resolution of the NTL data, the minimum distance between two sampling points is set as 1 km.

3. Results

3.1. Effectiveness of NDVI, EVI, NDBI, and POI in Reflecting NTL Distribution

In this study, the GDM is utilized to quantify the interpretation of RCNTL, NDVI, EVI, NDBI, and POI on the spatial distribution of NTL. As shown in Table 3, RCNTL unsurprisingly has the highest explanatory power. Apart from this, at the global scale (DN values (0, 63)), NDVI, EVI, NDBI, and POI all have a certain spatial correlation with the distributions of NTL. The q values were ordered as: NDBI (0.662) > EVI (0.593) > NDVI (0.531) > POI (0.473). This result indicates that the NDBI has the best performance in reflecting NTL distribution, followed by vegetation indices and POI. From the q values of EVI and NDVI, it can be seen that the explanatory power of the EVI is 11.6% higher than that of the NDVI. Compared with NDVI, the EVI has the advantage of overcoming easy saturation and attenuating soil background and atmospheric effects, and thus using the EVI to correct NTL data may be more effective than the NDVI. The results of the GDM further support the advantages of EVI. In the potential saturation region (DN value (53, 63)), it can be found that the NDBI and POI are more effective in reflecting the light intensity, especially the POI, which has almost doubled the explanatory power of the unsaturated region. For the unsaturation region (DN value (0, 52)), both NDBI and EVI can effectively depict the NTL distribution, while the POI has a relatively low explanatory power. This may be due to the lower density of POIs in suburban areas, which suggests that using POI density alone to regulate the NTL saturation problem may introduce a relatively large deviation into unsaturated areas.

Table 3. The results of the factor detector and interaction detector.

Light Intensity (DN)	Global Scale (DN Value (0, 63))	NTL Potential Saturation Region (DN Value (53, 63))	NTL Unsaturation Region (DN Value (0, 52))
RCNTL	0.694	0.637	0.602
NDBI	0.662	0.586	0.424
EVI	0.593	0.395	0.352
NDVI	0.531	0.303	0.371
POI	0.473	0.435	0.288
NDBI & EVI	0.744	0.583	0.550
NDBI & NDVI	0.681	0.490	0.502
NDBI & POI	0.797	0.842	0.653
EVI & NDVI	0.632	0.411	0.567
EVI & POI	0.751	0.526	0.418
NDVI & POI	0.694	0.585	0.496

Furthermore, the interaction detector is adopted to further measure the interaction effect of NDVI, EVI, NDBI, and POI on NTL spatial distribution. It is found that the interaction of NDVI, EVI, NDBI, and POI enhanced the explanatory power of the spatial distribution of NTL data. In particular, the largest q value at the global scale is NDBI

interacting with POI (0.797), which was 20.3% (NDBI) and 68.4% (POI) enhancement compared with their individual effect. Especially in the potential saturated region, the explanatory power is as high as 0.842. This illustrates the importance of the combination of NDBI and POI, which can effectively reflect the spatial distribution differences of NTL in the unsaturated and potential saturated regions. Therefore, it is highly feasible to combine NDBI and POI to construct the BPANTLI as a desaturation indicator to regulate the NTL saturation problem and delineate spatial differences in light intensity.

3.2. Desaturation Capacity of BPANTLI

In order to compare the characterization of light intensity by BPANTLI, this study selected the VANUI desaturation indicator in BTH urban agglomeration, the HSI desaturation indicator in YZD urban agglomeration, and the EANTLI desaturation indicator in PRD urban agglomeration, respectively, and compared their correction effects with BPANTLI. It can be clearly seen from Figures 6–8 that, compared with the original NTL DN value, the VANUI, EANTLI, and BPANTLI desaturation indicators can reduce the saturation effects and enhance the difference in light intensity within the potential saturation region. In the original NTL images, there is a clear saturation effect in the BTH, YZD, and PRD urban agglomerations. It is almost impossible to identify the internal light distribution. In general, the HSI-corrected results are slightly better than that of NTL, but cannot identify typical areas within cities. The calibration results of VANUI and EANTLI can better show the difference of light intensity in the saturated area, but there is little overall discrimination and it is difficult to distinguish typical areas. BPANTLI, on the other hand, can more effectively reduce the saturation problem and accurately delineate the differences in light intensity in saturation regions. The overall discrimination is much greater, and the typical plots in the saturation regions are easier to identify.

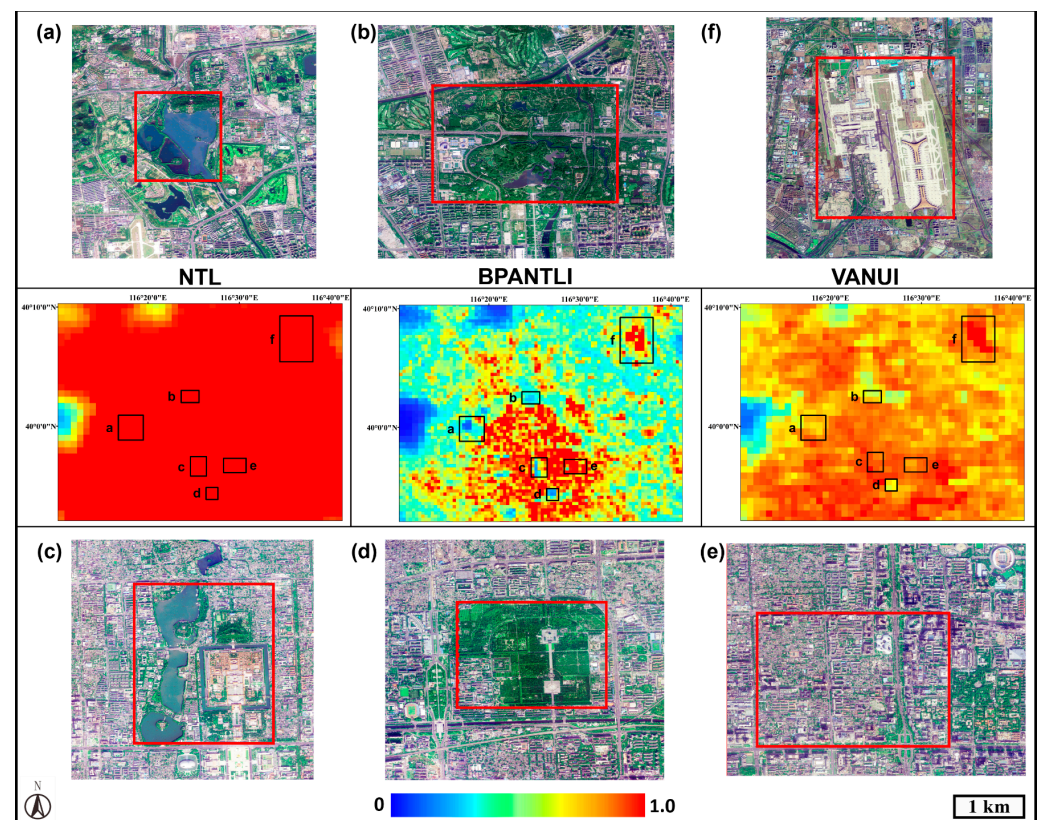


Figure 6. Comparison between NTL, BPANTLI, and VANUI in Beijing. (a) Summer Palace, (b) Olympic Park, (c) Forbidden City, (d) Temple of Heaven Park, (e) Beijing Economic Center, (f) Capital International Airport.

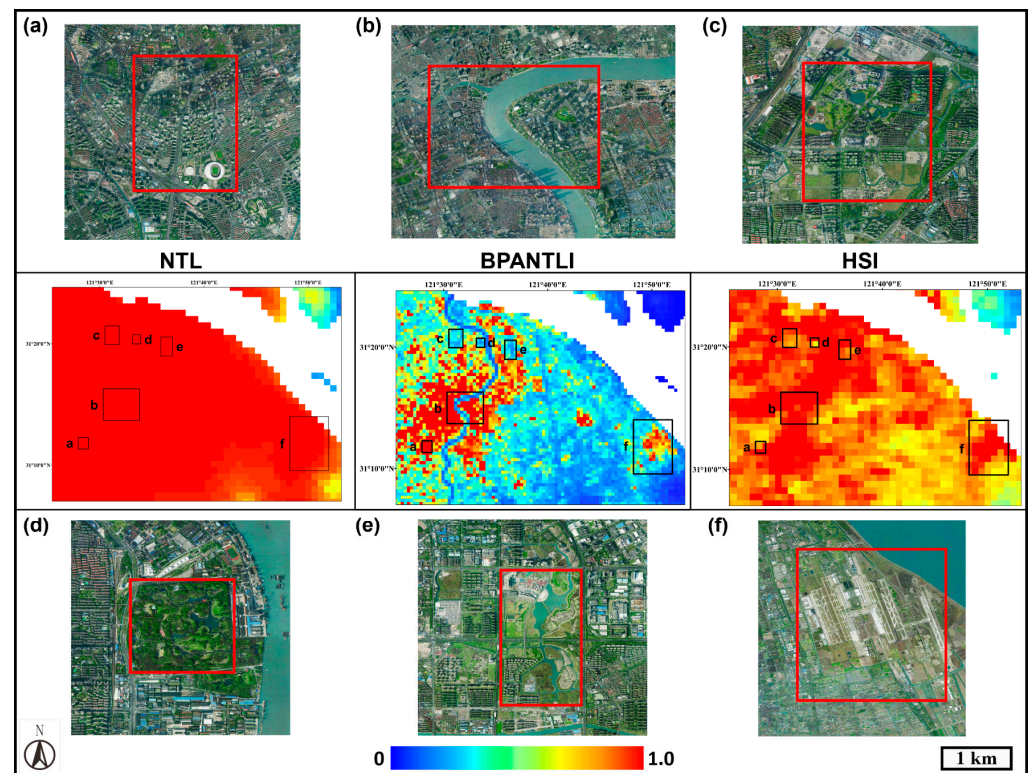


Figure 7. Comparison between NTL, BPANTLI, and HSI in Shanghai. (a) Xujiahui Commercial Zone, (b) Lujiazui CBD, (c) Jiangwan New City Park, (d) Gong-qing Forest Park, (e) Senlan Sports Park, (f) Pudong International Airport.

In BTH urban agglomeration (Figure 6), six typical plots located in Beijing were selected, namely: Summer Palace (a), Olympic Park (b), Forbidden City (c), Temple of Heaven Park (d), Beijing Economic Center (e), and Capital International Airport (f). In the original NTL images, none of the 6 typical plots can be identified. As for VANUI, the Olympic Park (b), Temple of Heaven (D), and Capital International Airport (f) can also be roughly recognized in VANUI, while other places cannot be distinguished due to insufficient contrast. However, in the BPANTLI, the above six plots are clearly identified. The difference between the light intensity and the surrounding area is clearly shown on the BPANTLI. For example, the Forbidden City (c) is closed at night (with weak light intensity), but due to its location in the center of Beijing, it is surrounded by bright lights at night.

In the YZD urban agglomeration (Figure 7), six typical areas located in Shanghai, namely: Xujiahui Commercial Zone (a), Lujiazui CBD (b), Jiangwan New City Park (c), Gongqing Forest Park (d), Senlan Sports Park (e), and Pudong International Airport (f) were selected. Similar to Figure 6, none of the six typical plots can be identified in the NTL map. In HSI, only Xujiahui Commercial Zone (a), Lujiazui CBD (b), and Pudong International Airport (f) can be identified. For the areas with more vegetation information, such as forests and parks, it is difficult for HSI to highlight the difference between these areas and the surrounding light intensity. This may be due to the error caused by the easy saturation of NDVI. In contrast, the BPANTLI can better identify various typical areas inside the saturation regions, where the Huangpu River, Lujiazui CBD, and Nanjing Road commercial areas are clearly distinguishable and the details of the rivers are not obscured. This result illustrates that the BPANTLI can accurately describe the differences in NTL intensity in saturation regions.

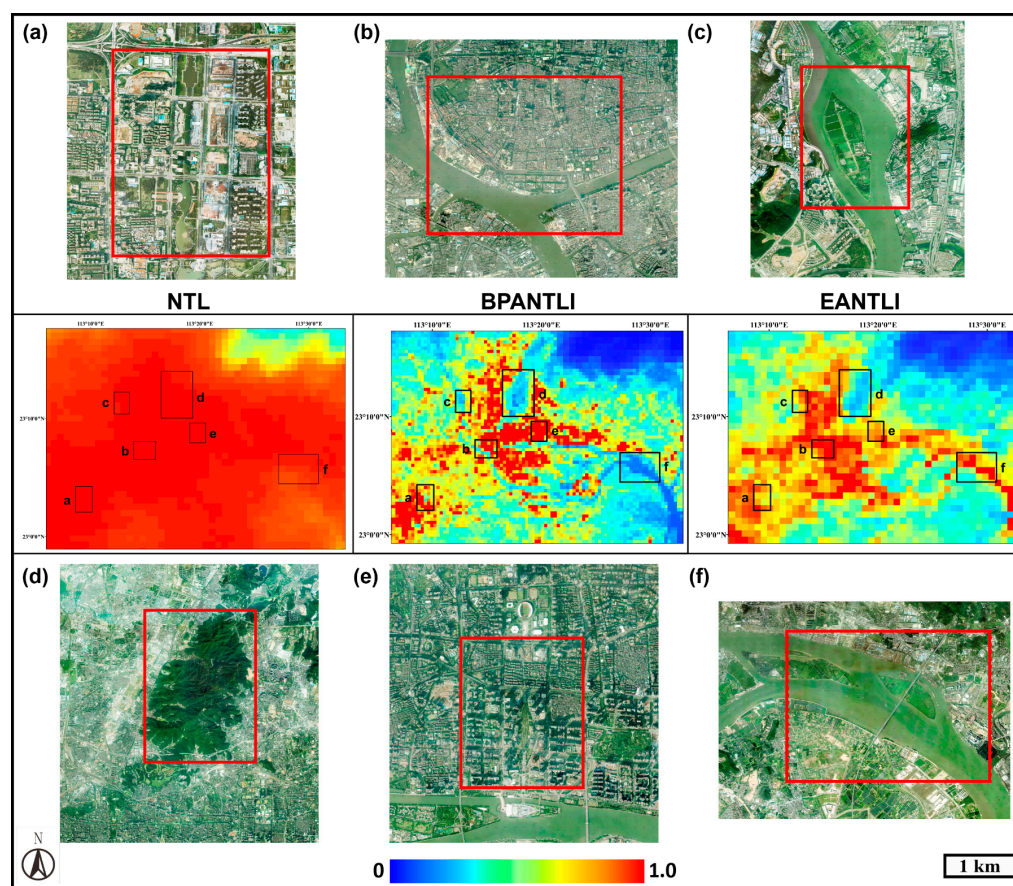


Figure 8. Comparison between NTL, BPANTLI, and EANTLI in PRD. (a) Foshan Financial High-tech Zone, (b) Guangzhou Liwan historical urban area, (c) Chenxiangsha river island, (d) Baiyun Mountain Scenic Area, (e) Zhujiang New Town CBD, (f) Pearl River Waterway.

In the PRD urban agglomeration, this study selected Foshan Financial High-tech Zone (a), Guangzhou Liwan historical urban area (b), Chenxiangsha river island (c), Baiyun Mountain Scenic Area (d), Zhujiang New Town CBD (e), and Pearl River Waterway (f). Similar to BTH and YZD urban agglomerations, the selected typical areas cannot be identified in the NTL data, whereas both EANTLI and BPANTLI can better distinguish these typical areas. However, it is difficult for EANTLI to recognize water body plots (c, f), which is mainly due to the fact that EANTLI is established based on the EVI that responds to the degree of vegetation coverage. The EVI values for both water bodies and built-up areas are relatively low, which leads to high EANTLI and an inability to distinguish between water bodies and urban centers. Thereby, the NTL intensity is similar between water bodies and built-up areas. Moreover, as for the area (a, e) of Foshan Financial High-tech Zone and Zhujiang New Town CBD, with a better understanding of sustainable urban development, the vegetation coverage in the urban CBD is gradually increasing, leading to low EANTLI values and underestimation of the NTL intensity of the CBD. In contrast, the BPANTLI better identifies these selected typical areas. The establishment of BPANTLI based on NDBI and POI can more accurately reflect the difference in light intensity within urban CBDs as well as in the suburbs.

3.3. Similarity between BPANTLI and RCNTL and NPP/VIIRS Data

As shown in Figure 9, three transect lines that pass through the potential saturation areas of the BTH, YZD, and PRD urban agglomerations are selected to visually compare the differences between NTL, EANTLI, BPANTLI, and RCNTL of each pixel. It can be seen that the NTL curve has a DN value of almost one as it passes through the city center. This result illustrates that the uncorrected NTL data has a significant saturation problem in the

city center, which does not characterize the details of the light intensity inside the saturated zone. However, the radiation-corrected RCNTL does not suffer from this problem. By comparing the fluctuation trends between the EANTLI, BPANTLI, and RCNTL curves, it can be seen that the BPANTLI and RCNTL curves fluctuate most similarly in both the potential saturation and unsaturated regions.

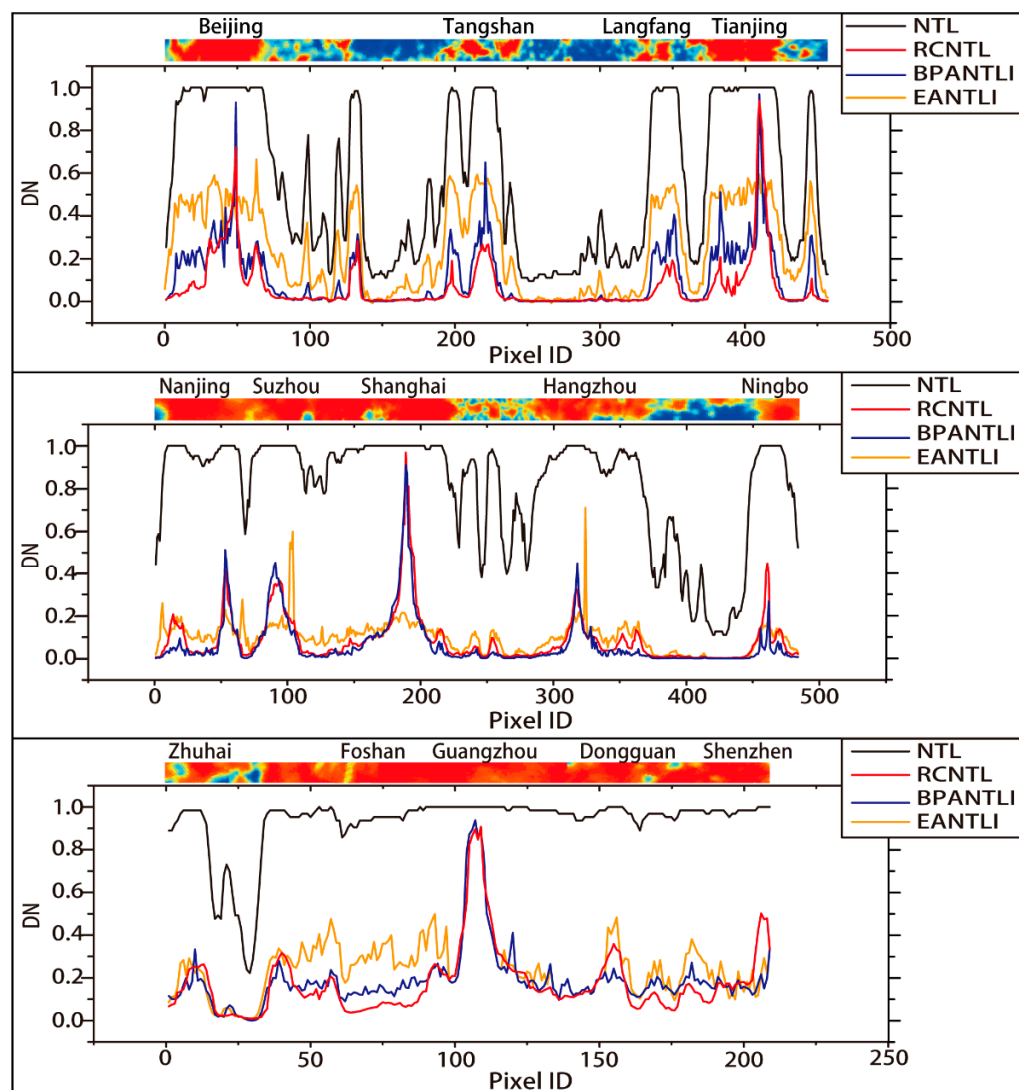


Figure 9. Transects of NTL, RCNTL, EANTLI, and BPANTLI in the BTH, YZD, and PRD urban agglomerations.

In order to further quantify the desaturation effect of BPANTLI, this study performed regression analysis on desaturation indicators (HSI, VANUI, EANTLI, BPANTLI) with RCNTL and NPP/VIIRS data to examine the similarity among them (Figure 10). It can be found that the fitting degree between BPANTLI and RCNTL, and NPP/VIIRS data is better than the other desaturation indicators ($EANTLI > VANUI > HSI$) in the BTH, YZD, PRD urban agglomerations, whether in the saturated or unsaturated areas, with a coefficient of determination R^2 greater than 0.80. This indicates that the BPANTLI-corrected light intensity has a more prominent correspondence correlation with NPP/VIIRS data, which further confirms the feasibility of the BPANTLI. Furthermore, the determination coefficient R^2 of EANTLI is higher than that of VANUI to varying degrees, which further confirms the superiority of EANTLI over VANUI in regulating NTL saturation problems. The fitting

degree of HSI and NPP/VIIRS data was the lowest, which further validates the results in Section 3.2.

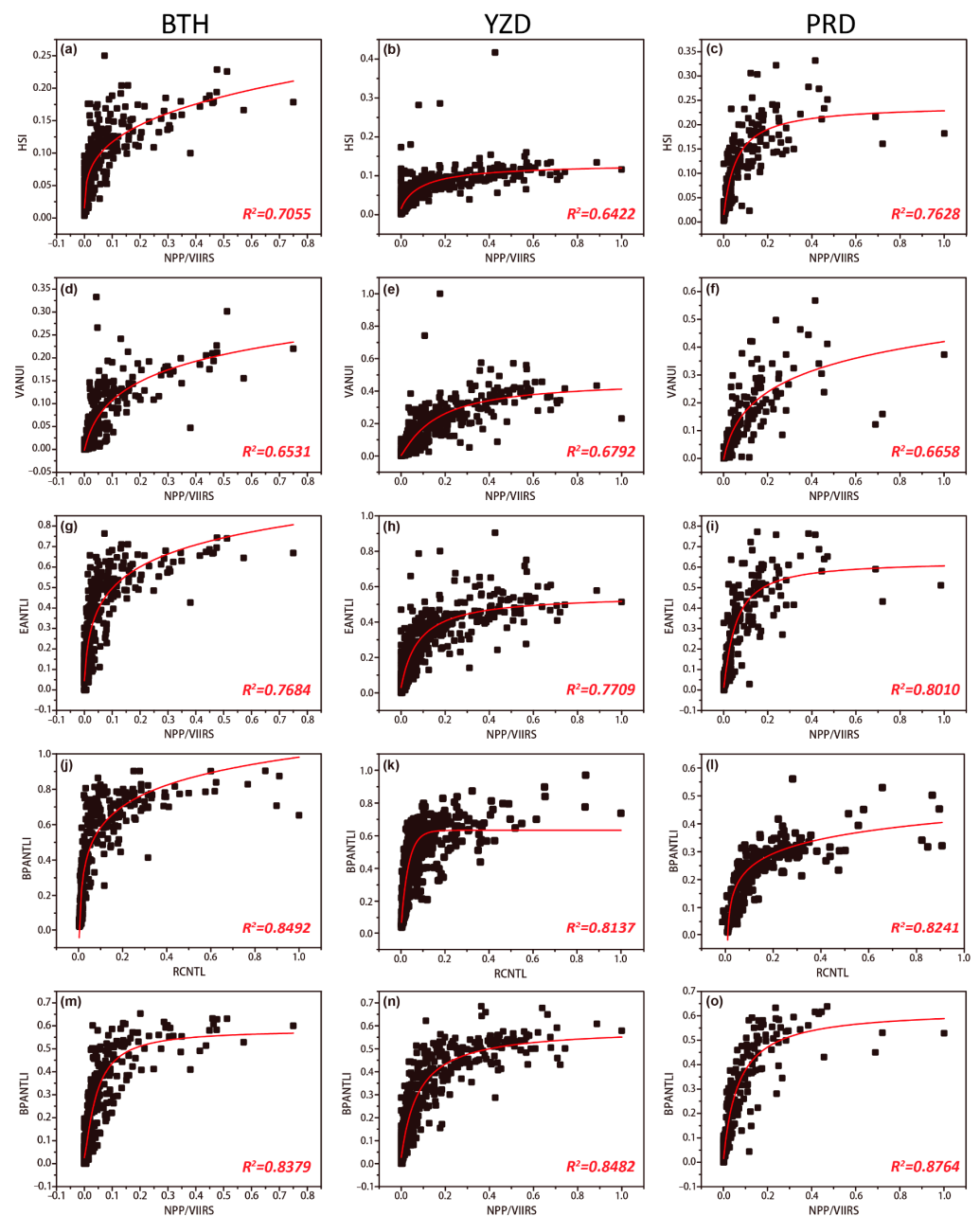


Figure 10. The fitting degree of HSI (a–c), VANUI (d–f), EANTLI (g–i), BPANTLI (j–o) with RCNTL and NPP/VIIRS.

3.4. Electricity Consumption, GDP, and Population Density Estimation

To verify the estimated accuracy of each desaturation indicator on regional electricity consumption (EC), GDP, and population density (PD), Figure 11 shows the regression results of the desaturation indicators (VANUI, EANTLI, BPANTLI) and NPP/VIIRS data in three urban agglomerations. We found that the NPP/VIIRS data obtain the highest correlation with all socio-economic indicators, especially population density, with an adjusted R^2 of 0.89. Compared with the original NTL data, the correlations of each desaturation indicator (VANUI, EANTLI, BPANTLI) with EC, GDP, and PD have increased significantly. This finding indicates that the desaturated NTL data allows for more accurate estimates of regional electricity consumption, GDP, and population density. More importantly, the

fitting degree of BPANTLI for electricity consumption, GDP, and population density is significantly higher than other indicators and is not much different from NPP/VIIRS data. In detail, the adjusted R^2 of BPANTLI and EC is as high as 0.81, which is 15.0% and 11.3% higher than the R^2 of EANTLI and VANUI, respectively. The regression coefficient between BPANTLI and GDP is 0.76, followed by EANTLI (0.74), and VANUI (0.73). As for population density, the R^2 of BPANTLI is 0.86, which has a significant advantage over the EANTLI, VANUI, and NTL. Additionally, compared with the NPP/VIIRS data, the fitting degree among BPANTLI and EC, GDP, and PD is only 3.3%, 8.8%, and 3.1% lower than NPP/VIIRS data. In other words, there is a certain corresponding correlation among them. This result suggests that the BPANTLI-regulated light intensity provides better accuracy for estimating electricity consumption, GDP, and population density.

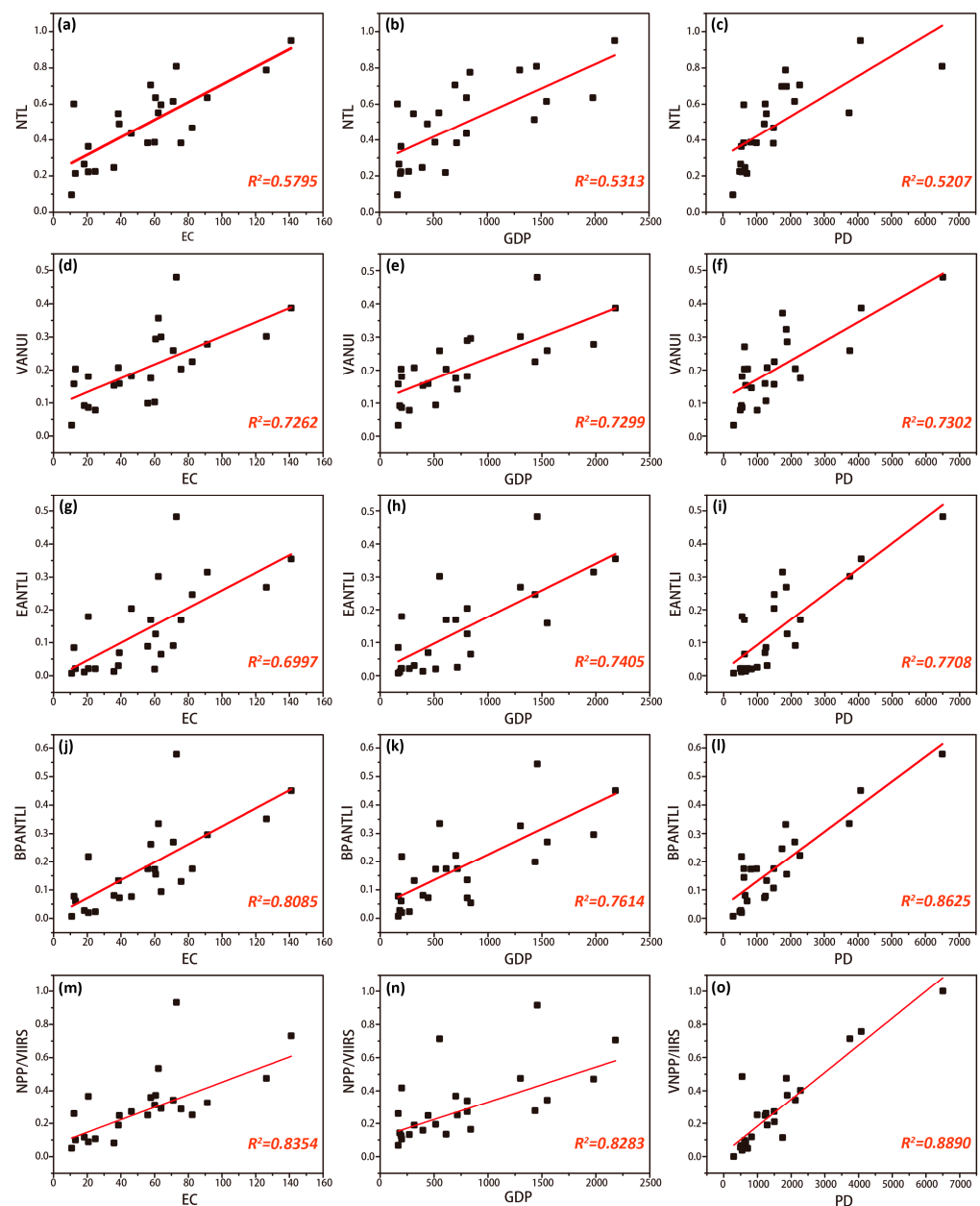


Figure 11. Regression analysis of the NTL (a–c), VANUI (d–f), EANTLI (g–i), BPANTLI (j–l), and NPP/VIIRS (m–o) with the EC, GDP, and PD at the prefecture level.

Furthermore, given the highly corresponding correlation of population density, this study randomly selected 500 sample points in five cities of Beijing, Shanghai, Guangzhou,

Shenzhen, and Foshan to verify the accuracy of the BPANTLI index for estimating population density at the pixel level. As shown in Figure 12, at the pixel level, the fitting coefficients of BPANTLI with population density in Beijing, Shanghai, Guangzhou, and Shenzhen are 0.80, 0.78, 0.83, 0.75, and 0.69, respectively, which are significantly higher than those of EANTLI and VANUI. Similarly, the NPP/VIIRS data also obtain the highest fitting degree with population density at the pixel level in these five cities. Therefore, it can be seen that, not only at the city level, the BPANTLI-corrected light intensity also has better accuracy for the population density estimation at the pixel level.

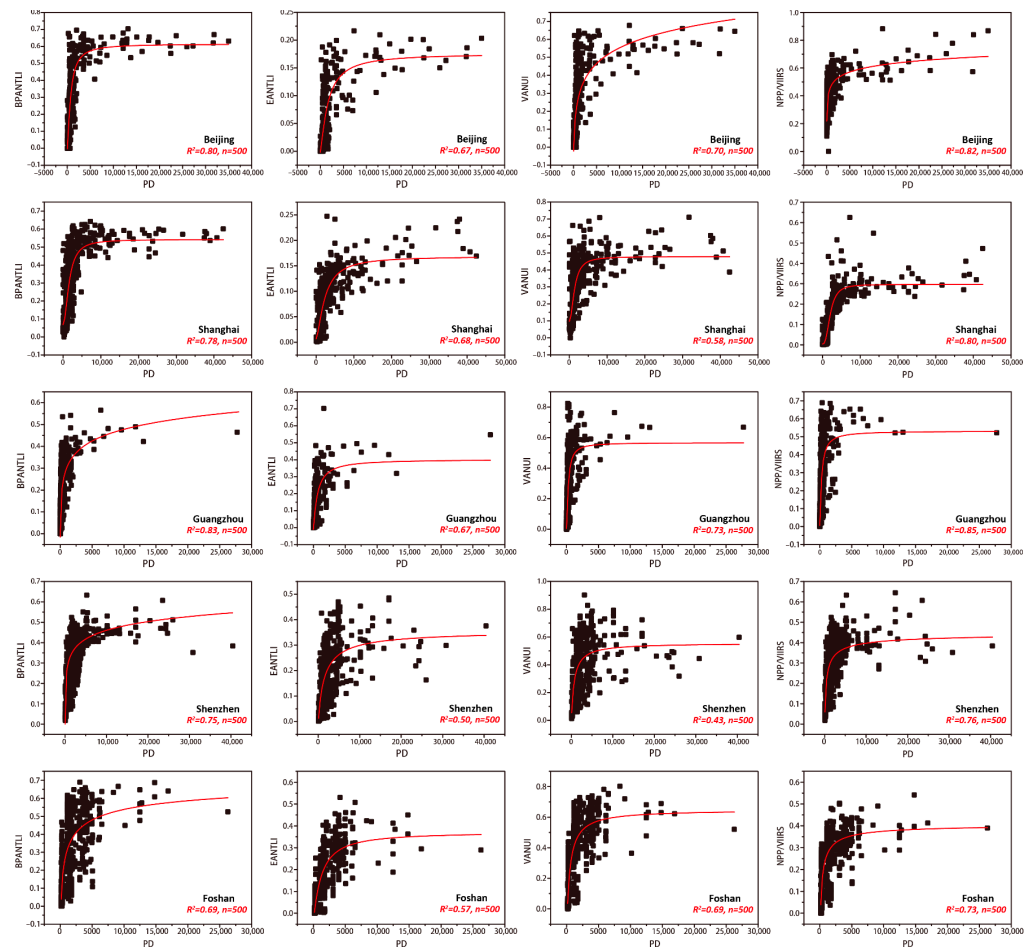


Figure 12. Regression analysis of BPANTLI and population density at the pixel level in Beijing, Shanghai, Guangzhou, Shenzhen, and Foshan city.

4. Discussion

4.1. Evaluate the Desaturation Effect of Each Indicator

The desaturation effect of NTL data is inextricably linked to the construction of the desaturation indicator. Previous studies utilize NDVI or EVI to construct desaturation indicators (HSI, VANUI, EANTLI) under the assumption that light intensity is inversely proportional to vegetation coverage [34,35,57,58]. However, we have noticed that this negative correlation is not very stable, especially in rapidly urbanizing areas. Firstly, rapid urbanization has led to a dramatic decline in urban vegetation density. The continuous encroachment of urban green space leads to the fragmentation of the vegetation landscape and inhibits the spatial heterogeneity of vegetation coverage. Using vegetation coverage with low spatial heterogeneity to regulate saturated NTL data may lead to the inability to depict the spatial distribution differences in light intensity (Figures 6–8). Secondly, with the introduction of concepts such as sustainable urban development and habitable cities, the vegetation abundance within CBDs is gradually increasing. Therefore, using the

vegetation-based desaturation indicator will undoubtedly underestimate the light intensity of the CBD at night (Figure 7). Thirdly, in certain areas, it is difficult to use vegetation coverage to characterize light intensity. For example, the vegetation coverage of water bodies or bare land is relatively low (low NDVI or EVI), but this does not mean that the light intensity is high (Figure 8). Based on this assumption, the relatively low NDVI and EVI values incorrectly increase the light intensity in these areas. Moreover, this error is even more pronounced when these areas are located on the urban fringe. It is worth noting that vegetation cover in some desert cities does not show a trend of being low in urban centers and high in suburban areas. These desert cities are constantly increasing their vegetation coverage in order to adapt to the demands for livability. Therefore, the assumption that NTL intensity is inversely related to vegetation abundance may not be applicable to these cities.

It is well known that light intensity is closely related to economic vitality and human activities [59,60]. That is to say, light intensity is more of a socio-economic indicator reflecting human activity. However, the vegetation index is only a side reflection of socio-economic intensity, which assumes urban development will encroach on vegetation coverage. In reality, a place with sparse vegetation often does not imply strong socio-economic vitality in the area. This also explains the defect of using vegetation-based desaturation indicators alone to regulate NTL. Based on this, this study proposes a novel desaturation indicator based on the urban spatial structure and socio-economic activity intensity. With the development of the city, various urban facilities related to daily life become denser, along with a large proportion of urban built-up areas. At the same time, the light intensity is also increasing. This positive relationship is the theoretical basis for the BPANTLI correction method developed in this study. The GDM results (Table 3) further confirmed this conjecture that the combination of the NDBI and POI has the highest explanatory power for the spatial distribution of light intensity, whether in saturated or unsaturated regions. Thus, it is highly feasible to combine NDBI and POI to construct the BPANTLI as a desaturation indicator to regulate the NTL saturation problem and delineate light intensity. By comparing the desaturation results with HSI, VANUI, and EANTLI, the BPANTLI can more effectively reduce the saturation problem and express spatial differences in light intensity. We can easily distinguish the urban inner structures such as central business districts, green areas, airports, and river channels. Furthermore, the BPANTLI shows a more prominent similarity to radiation-calibrated data, with a much higher coefficient of determination R^2 than other indicators. This result illustrates the desaturation accuracy of BPANTLI, which depicts a more realistic picture of the light intensity distribution. Also, the BPANTLI-regulated light intensity significantly improves the accuracy of estimating urban socio-economic activity, which provides better reference data for electricity consumption, GDP, and population density estimates. In general, the validation results from the above three aspects fully demonstrate the effectiveness of the BPANTLI in regulating the NTL saturation problem. Therefore, the BPANTLI proposed in this study can be considered a reasonable indicator of NTL desaturation.

With the development of the remote sensing cloud computing platform (Google Earth Engine), the huge storage space and advanced cloud computing capabilities have made largescale desaturation studies possible. In this context, this study further applies the proposed BPANTLI method to the typical NTL saturation region in Asia, Europe, and North America (Figure 13).

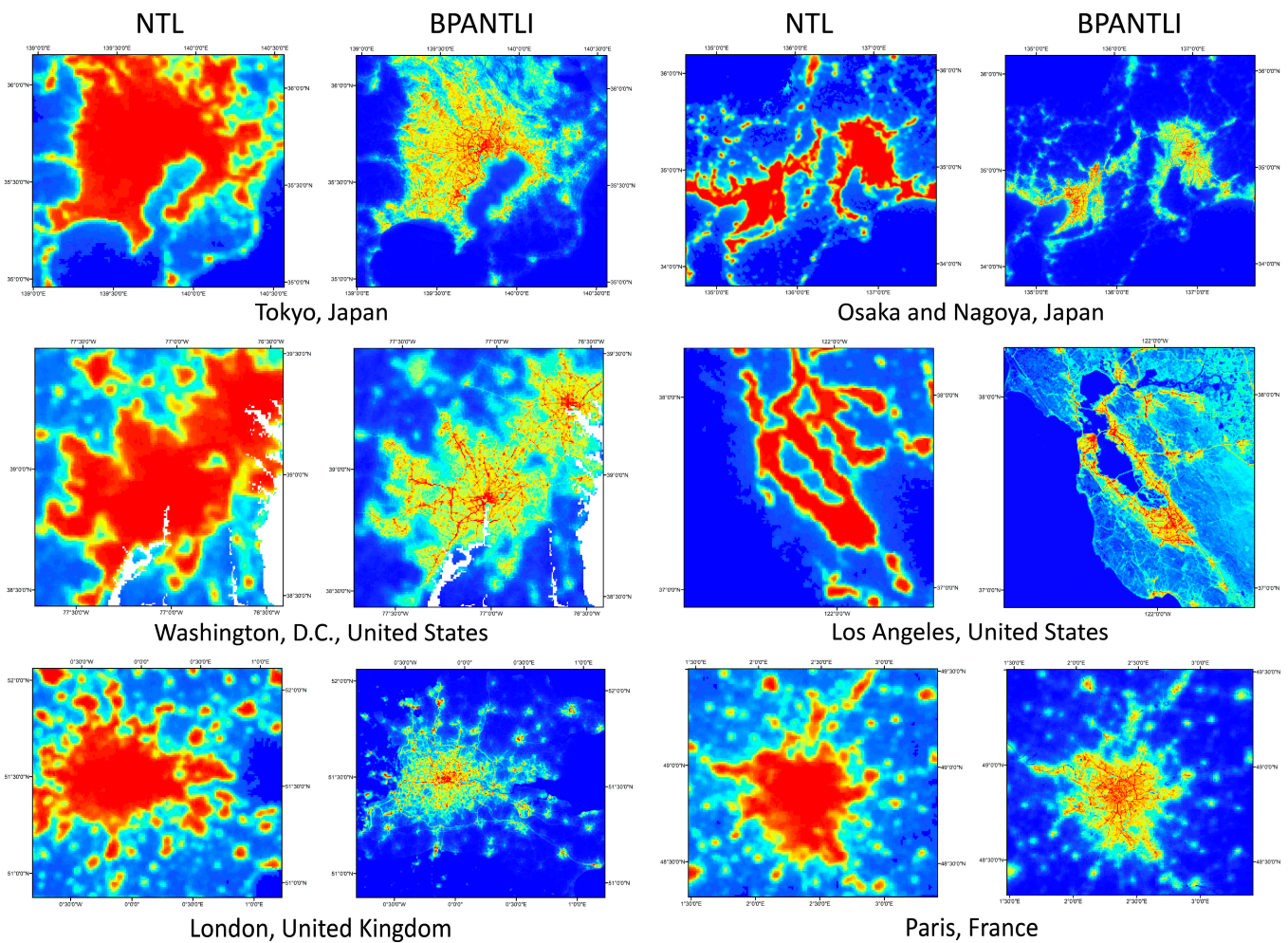


Figure 13. Comparison between DMSP/OLS NTL and BPANTLI in Tokyo, Osaka, Nagoya, Washington, D.C., Los Angeles, London, and Paris.

4.2. Overcoming the Spatial Resolution of NTL Data

It has become widely accepted that light data directly reflects human activity. Considerable research has been carried out using DMSP/OLS NTL data to estimate urban social and economic parameters (GDP, population, energy consumption), and to monitor urbanization processes and the ecological environment [61–65]. However, due to the generally low spatial resolution of DMSP/OLS NTL data, its application accuracy is greatly limited. With the development of nighttime observation technology, the spatial resolution of the NPP/VIIRS and Luojia 1 light data have been increased to 500 m and 130 m, respectively. Although the spatial resolution of NPP/VIIRS and Luojia 1 light data have now been significantly improved, these datasets have only become available in recent years. This implies these high-spatial-resolution NTL datasets cannot be used for long time-series studies. In contrast, given the long-term historical monitoring of DMSP/OLS NTL data, the unique ability to conduct long-term time series analysis exists. Therefore, it is of great practical significance to overcome the original spatial resolution of DMSP/OLS data to produce more accurate historical data. In view of the advantages of NDBI and POI vector data in spatial resolution, we can achieve dynamic conversion of BPANTLI spatial resolution by setting grid units with different sizes according to research needs, thus breaking through the limitation of DMSP/OLS NTL data spatial resolution (Figure 14). For example, in this study, the spatial resolution of BPANTLI-regulated NTL data is 500 m (Figure 4). We can even set the grid size to 250 m for higher spatial resolution light intensity. On the contrary, since the spatial resolution of NDVI and EVI of MOD13A3 products is

1 km (similar resolution with light intensity), whose inherent spatial resolution is difficult to improve. The BPANTLI-regulated light data with a higher spatial resolution allows for a better characterization of the spatial distribution differences of light intensity, which is expected to produce more accurate and meaningful regulated results.

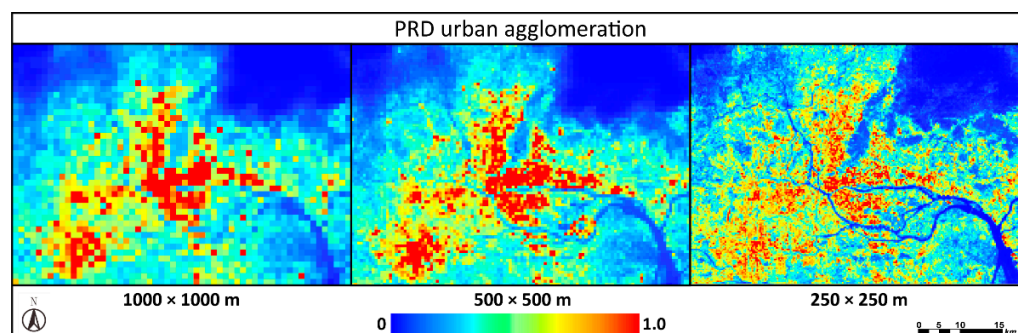


Figure 14. The multi-level spatial resolution of BPANTLI.

However, it is important to note that this method cannot improve the spatial resolution to a relatively high level (50 m, 100 m). Theoretically, we can increase the spatial resolution of BPANTLI up to 30 m (based on NDBI resolution), but the spatial resolution of the original DMSP/OLS NTL data is still 1 km. Simply building higher resolution grid units (i.e., 30 m) to increase the spatial resolution of BPANTLI while maintaining the same resolution of the original NTL data (still 1 km) will inevitably create more uncertainty (excessive spatial heterogeneity). As shown in Table 4, we found that the correlation between BPANTLI and NPP/VIIRS began to decline at a spatial resolution of 100 meters. Therefore, this result suggests that the method proposed in this study can only improve the spatial resolution of nighttime light to a certain extent.

Table 4. The fitting degree between BPANTLI and NPP/VIIRS data across different spatial resolutions in Guangzhou.

NPP/VIIRS	BPANTLI					
	Spatial resolution	250 m	200 m	100 m	50 m	30 m
Correlation coefficient		0.75	0.78	0.67	0.62	0.54

4.3. Limitations

Although the BPANTLI proposed in this study has many advantages, there are still some shortcomings that should be considered in future work. Firstly, in this study, we only considered the POI density within each grid unit and did not distinguish the differences in light emission of the selected POI types (commercial, entertainment, dining, and residential). Therefore, the light emission of different POIs should be further considered in order to delineate the actual light intensities in more detail. Secondly, for the principle of BPANTLI, this study develops the BPANTLI only based on the results of interactive detectors of the geographical detector model. Hence, the sensitivity analysis of the proposed method needs to be further supplemented in following research. Thirdly, the BPANTLI is established based on NDBI and POI, so the difficulty of obtaining NDBI and POI will directly affect the application of this desaturation method. Compared with the NDVI and EVI vegetation indices that can be directly obtained from MODIS MOD13A3 products, the development of BPANTLI first needs to calculate NDBI and POI density, which undoubtedly increases the difficulty of applying the BPANTLI desaturation indicator. With the explosive growth of spatiotemporal geographic data, the time required to update multi-source remote sensing data and POI has become shorter, providing a data basis for the construction of BPANTLI desaturation models. In addition, with the development of the remote sensing cloud

computing platform (Google Earth Engine), the huge storage space and advanced cloud computing capabilities have made large-scale desaturation studies possible. Lastly, only one year and three major urban agglomerations are selected to verify the effectiveness of the BPANTLI in reducing the NTL saturation problem. Therefore, it is necessary to further construct long-term series and cross-regional BPANTLI data to further verify its universality and credibility.

5. Conclusions

In this study, a novel desaturation indicator, BPANTLI, that combines NDBI and POI is proposed to regulate the DMSP/OLS NTL saturation problem based on the spatial characteristics of urban structures and human activity. The geographical detector model is firstly adopted to quantify the explanatory power of NDVI, EVI, NDBI, and POI on light intensity distribution, so as to clarify the feasibility of developing the BPANTLI desaturation indicator. The performance and applicability of BPANTLI are validated in three major urban agglomerations with the most severe light saturation problems in China through the depiction of light intensity spatial differences in NTL saturation regions; the similarity among the BPANTLI and the RCNTL, NPP/VIIRS data; and the accuracy of estimating urban socio-economic parameters (electricity consumption, GDP, population density). The results indicate that compared with HSI, VANUI, and EANTLI desaturation indicators, the BPANTLI can robustly and effectively regulate the NTL saturation problem and delineate the spatial differences of light intensity. In the potential saturation region of three urban agglomerations, the typically selected areas that are indistinguishable in the original NTL and HSI or difficult to distinguish in the VANUI and EANTLI can be clearly distinguished in the BPANTLI-regulated NTL data. Secondly, the BPANTLI shows a more prominent similarity with RCNTL and NPP/VIRRS data, with a much higher coefficient of determination R^2 than other indicators. Thirdly, the BPANTLI-regulated light intensity significantly improves the accuracy of estimating urban socio-economic activity, which provides a better reference data for electricity consumption, GDP, and population density estimates. Overall, the results of these three aspects confirm that the BPANTLI proposed in this study can more effectively alleviate the saturation problem and delineate a more realistic picture of the light intensity distribution. Through the construction of the BPANTLI, the existing DMSP/OLS NTL data can be desaturated and regulated to obtain a time-series-calibrated NTL dataset, which can compensate for the deficiencies of the radiation calibration NTL data (RCNTL). At the same time, the dynamic conversion of the spatial resolution of nighttime light data can also be realized according to the research needs, so as to more accurately characterize the spatial distribution difference of light intensity and provide an accurate data set for research requiring NTL data.

Author Contributions: Conceptualization, Q.Z. and Z.Z.; methodology, Q.Z. and Z.Z.; software, Q.Z.; validation, Q.Z., Z.Z. and Z.C.; formal analysis, Q.Z. and Z.Z.; investigation, Q.Z.; resources, Z.W.; data curation, Q.Z.; writing—original draft preparation, Q.Z.; writing—review and editing, Q.Z. and Z.Z.; visualization, R.L.; supervision, Z.W. and Z.C.; project administration, Z.W.; funding acquisition, Z.W. All authors have read and agreed to the published version of the manuscript.

Funding: This research was funded by the Key Special Project for Introduced Talents Team of Southern Marine Science and Engineering Guangdong Laboratory (Guangzhou) (No. GML2019ZD0301); the NSFC-Guangdong Joint Foundation Key Project (U1901219); and the National Natural Science Foundation of China (41801250).

Data Availability Statement: The remote sensing data and code used in this study are openly available on the website.

Acknowledgments: The authors are grateful for the comments and suggestions provided by reviewers and editors.

Conflicts of Interest: The authors declare no conflict of interest.

References

1. Ma, T.; Zhou, C.; Pei, T.; Haynie, S.; Fan, J. Quantitative estimation of urbanization dynamics using time series of DMSP/OLS nighttime light data: A comparative case study from China's cities. *Remote Sens. Environ.* **2012**, *124*, 99–107. [[CrossRef](#)]
2. Gao, B.; Huang, Q.; He, C.; Ma, Q. Dynamics of urbanization levels in China from 1992 to 2012: Perspective from DMSP/OLS nighttime light data. *Remote Sens.* **2015**, *7*, 1721–1735. [[CrossRef](#)]
3. Zhao, M.; Cheng, W.; Zhou, C.; Li, M.; Huang, K.; Wang, N. Assessing spatiotemporal characteristics of urbanization dynamics in Southeast Asia using time series of DMSP/OLS nighttime light data. *Remote Sens.* **2018**, *10*, 47. [[CrossRef](#)]
4. Xu, Z.; He, X.; Chen, L.; Hu, X.; Tang, W.; Li, J. How does the urbanization level change in the Yangtze River economic belt, China? A Multi-Scale Evaluation Using DMSP/OLS Nighttime Light Data. In *IOP Conference Series: Earth and Environmental Science*; IOP Publishing: Bristol, UK, 2021; Volume 675, p. 012112.
5. Xu, P.; Lin, M.; Jin, P. Spatio-temporal Dynamics of Urbanization in China Using DMSP/OLS Nighttime Light Data from 1992–2013. *Chin. Geogr. Sci.* **2021**, *31*, 70–80. [[CrossRef](#)]
6. Hu, Y.N.; Peng, J.; Liu, Y.; Du, Y.; Li, H.; Wu, J. Mapping development pattern in Beijing-Tianjin-Hebei urban agglomeration using DMSP/OLS nighttime light data. *Remote Sens.* **2017**, *9*, 760. [[CrossRef](#)]
7. Xu, T.; Ma, T.; Zhou, C.; Zhou, Y. Characterizing spatio-temporal dynamics of urbanization in China using time series of DMSP/OLS night light data. *Remote Sens.* **2014**, *6*, 7708–7731. [[CrossRef](#)]
8. Zhang, Q.; Seto, K.C. Mapping urbanization dynamics at regional and global scales using multi-temporal DMSP/OLS nighttime light data. *Remote Sens. Environ.* **2011**, *115*, 2320–2329. [[CrossRef](#)]
9. Liu, Y.; Wang, Y.; Peng, J.; Du, Y.; Liu, X.; Li, S.; Zhang, D. Correlations between urbanization and vegetation degradation across the world's metropolises using DMSP/OLS nighttime light data. *Remote Sens.* **2015**, *7*, 2067–2088. [[CrossRef](#)]
10. Xie, Y.; Weng, Q. World energy consumption pattern as revealed by DMSP-OLS nighttime light imagery. *Gisci. Remote Sens.* **2016**, *53*, 265–282. [[CrossRef](#)]
11. Lv, Q.; Liu, H.; Wang, J.; Liu, H.; Shang, Y. Multiscale analysis on spatiotemporal dynamics of energy consumption CO2 emissions in China: Utilizing the integrated of DMSP-OLS and NPP-VIIRS nighttime light datasets. *Sci. Total Environ.* **2020**, *703*, 134394. [[CrossRef](#)]
12. Yue, Y.; Tian, L.; Yue, Q.; Wang, Z. Spatiotemporal variations in energy consumption and their influencing factors in China based on the integration of the DMSP-OLS and NPP-VIIRS nighttime light datasets. *Remote Sens.* **2020**, *12*, 1151. [[CrossRef](#)]
13. Shi, K.; Yu, B.; Huang, Y.; Hu, Y.; Yin, B.; Chen, Z.; Chen, L.; Wu, J. Evaluating the ability of NPP-VIIRS nighttime light data to estimate the gross domestic product and the electric power consumption of China at multiple scales: A comparison with DMSP-OLS data. *Remote Sens.* **2014**, *6*, 1705–1724. [[CrossRef](#)]
14. Wu, J.; Wang, Z.; Li, W.; Peng, J. Exploring factors affecting the relationship between light consumption and GDP based on DMSP/OLS nighttime satellite imagery. *Remote Sens. Environ.* **2013**, *134*, 111–119. [[CrossRef](#)]
15. Fu, H.; Shao, Z.; Fu, P.; Cheng, Q. The dynamic analysis between urban nighttime economy and urbanization using the DMSP/OLS nighttime light data in China from 1992 to 2012. *Remote Sens.* **2017**, *9*, 416. [[CrossRef](#)]
16. Tripathy, B.R.; Tiwari, V.; Pandey, V.; Elvidge, C.D.; Rawat, J.S.; Sharma, M.P.; Prawasi, R.; Kumar, P. Estimation of urban population dynamics using DMSP-OLS night-time lights time series sensors data. *IEEE Sens. J.* **2016**, *17*, 1013–1020. [[CrossRef](#)]
17. Kumar, P.; Sajjad, H.; Joshi, P.K.; Elvidge, C.D.; Rehman, S.; Chaudhary, B.S.; Tripathy, B.R.; Singh, J.; Pipal, G. Modeling the luminous intensity of Beijing, China using DMSP-OLS night-time lights series data for estimating population density. *Phys. Chem. Earth* **2019**, *109*, 31–39. [[CrossRef](#)]
18. Shi, K.; Huang, C.; Yu, B.; Yin, B.; Huang, Y.; Wu, J. Evaluation of NPP-VIIRS night-time light composite data for extracting built-up urban areas. *Remote Sens. Lett.* **2014**, *5*, 358–366. [[CrossRef](#)]
19. Yu, B.; Shi, K.; Hu, Y.; Huang, C.; Chen, Z.; Wu, J. Poverty evaluation using NPP-VIIRS nighttime light composite data at the county level in China. *IEEE J. Sel. Top. Appl. Earth Observ. Remote Sens.* **2015**, *8*, 1217–1229. [[CrossRef](#)]
20. Sahoo, S.; Gupta, P.K.; Srivastav, S.K. Comparative analysis between VIIRS-DNB and DMSP-OLS night-time light data to estimate electric power consumption in Uttar Pradesh, India. *Int. J. Remote Sens.* **2020**, *41*, 2565–2580. [[CrossRef](#)]
21. Zheng, Y.; He, Y.; Zhou, Q.; Wang, H. Quantitative Evaluation of Urban Expansion using NPP-VIIRS Nighttime Light and Landsat Spectral Data. *Sustain. Cities Soc.* **2022**, *76*, 103338. [[CrossRef](#)]
22. Pok, S.; Matsushita, B.; Fukushima, T. An easily implemented method to estimate impervious surface area on a large scale from MODIS time-series and improved DMSP-OLS nighttime light data. *ISPRS J. Photogramm.* **2017**, *133*, 104–115. [[CrossRef](#)]
23. Cao, X.; Hu, Y.; Zhu, X.; Shi, F.; Zhuo, L.; Chen, J. A simple self-adjusting model for correcting the blooming effects in DMSP-OLS nighttime light images. *Remote Sens. Environ.* **2019**, *224*, 401–411. [[CrossRef](#)]
24. Shen, Z.; Zhu, X.; Cao, X.; Chen, J. Measurement of blooming effect of DMSP-OLS nighttime light data based on NPP-VIIRS data. *Ann. GIS* **2019**, *25*, 153–165. [[CrossRef](#)]
25. Elvidge, C.D.; Baugh, K.E.; Dietz, J.B.; Bland, T.; Sutton, P.C.; Kroehl, H.W. Radiance calibration of DMSP-OLS low-light imaging data of human settlements. *Remote Sens. Environ.* **1999**, *68*, 77–88. [[CrossRef](#)]
26. Guo, W.; Lu, D.; Kuang, W. Improving fractional impervious surface mapping performance through combination of DMSP-OLS and MODIS NDVI data. *Remote Sens.* **2017**, *9*, 375. [[CrossRef](#)]
27. Hsu, F.C.; Baugh, K.E.; Ghosh, T.; Zhizhin, M.; Elvidge, C.D. DMSP-OLS radiance calibrated nighttime lights time series with intercalibration. *Remote Sens.* **2015**, *7*, 1855–1876. [[CrossRef](#)]

28. Hu, Y.; Chen, J.; Cao, X.; Chen, X.; Cui, X.; Gan, L. Correcting the Saturation Effect in DMSP/OLS Stable Nighttime Light Products Based on Radiance-Calibrated Data. *IEEE Trans. Geosci. Remote Sens.* **2021**, *60*, 5602011. [[CrossRef](#)]
29. Huang, X.; Shi, K.; Cui, Y.; Li, Y. A saturated light correction method for DMSP-OLS nighttime stable light data by remote and social sensing data. *IEEE J. Sel. Top. Appl. Earth Observ. Remote Sens.* **2021**, *14*, 1885–1894. [[CrossRef](#)]
30. Cao, Z.; Wu, Z.; Kuang, Y.Q.; Huang, N. Correction of DMSP/OLS night-time light images and its application in China. *J. Geo-Inf. Sci.* **2015**, *17*, 1092–1102.
31. Letu, H.; Hara, M.; Yagi, H.; Naoki, K.; Tana, G.; Nishio, F.; Shuhei, O. Estimating energy consumption from night-time DMPS/OLS imagery after correcting for saturation effects. *Int. J. Remote Sens.* **2010**, *31*, 4443–4458. [[CrossRef](#)]
32. Letu, H.; Hara, M.; Tana, G.; Nishio, F. A saturated light correction method for DMSP/OLS nighttime satellite imagery. *IEEE Trans. Geosci. Remote Sens.* **2011**, *50*, 389–396. [[CrossRef](#)]
33. Lu, D.; Tian, H.; Zhou, G.; Ge, H. Regional mapping of human settlements in southeastern China with multisensor remotely sensed data. *Remote Sens. Environ.* **2008**, *112*, 3668–3679. [[CrossRef](#)]
34. Zhang, Q.; Schaaf, C.; Seto, K.C. The vegetation adjusted NTL urban index: A new approach to reduce saturation and increase variation in nighttime luminosity. *Remote Sens. Environ.* **2013**, *129*, 32–41. [[CrossRef](#)]
35. Zhuo, L.; Zhang, X.; Zheng, J.; Tao, H.; Guo, Y. An EVI-based method to reduce saturation of DMSP/OLS nighttime light data. *Acta Geogr. Sin.* **2015**, *70*, 1339–1350.
36. Meng, X.; Han, J.; Huang, C. An improved vegetation adjusted nighttime light urban index and its application in quantifying spatiotemporal dynamics of carbon emissions in China. *Remote Sens.* **2017**, *9*, 829. [[CrossRef](#)]
37. Liu, Y.; Yang, Y.; Jing, W.; Yao, L.; Yue, X.; Zhao, X. A new urban index for expressing inner-city patterns based on MODIS LST and EVI regulated DMSP/OLS NTL. *Remote Sens.* **2017**, *9*, 777. [[CrossRef](#)]
38. Zheng, Z.; Chen, Y.; Wu, Z.; Ye, X.; Guo, G.; Qian, Q. The desaturation method of DMSP/OLS nighttime light data based on vector data: Taking the rapidly urbanized China as an example. *Int. J. Geograph. Inf. Sci.* **2019**, *33*, 431–453. [[CrossRef](#)]
39. He, D.; Shi, Q.; Liu, X.; Zhong, Y.; Zhang, L. Generating 2 m fine-scale urban tree cover product over 34 metropolises in China based on deep context-aware sub-pixel mapping network. *Int. J. Appl. Earth Obs.* **2022**, *106*, 102667. [[CrossRef](#)]
40. Zha, Y.; Gao, J.; Ni, S. Use of normalized difference built-up index in automatically mapping urban areas from TM imagery. *Int. J. Remote Sens.* **2003**, *24*, 583–594. [[CrossRef](#)]
41. Varshney, A.; Rajesh, E. A comparative study of built-up index approaches for automated extraction of built-up regions from remote sensing data. *J. Indian Soc. Remote Sens.* **2014**, *42*, 659–663. [[CrossRef](#)]
42. Guha, S.; Govil, H.; Dey, A.; Gill, N. Analytical study of land surface temperature with NDVI and NDBI using Landsat 8 OLI and TIRS data in Florence and Naples city, Italy. *Eur. J. Remote Sens.* **2018**, *51*, 667–678. [[CrossRef](#)]
43. Li, K.; Chen, Y. A Genetic Algorithm-based urban cluster automatic threshold method by combining VIIRS DNB, NDVI, and NDBI to monitor urbanization. *Remote Sens.* **2018**, *10*, 277. [[CrossRef](#)]
44. Jamei, Y.; Rajagopalan, P.; Sun, Q.C. Spatial structure of surface urban heat island and its relationship with vegetation and built-up areas in Melbourne, Australia. *Sci. Total Environ.* **2019**, *659*, 1335–1351. [[CrossRef](#)]
45. Guha, S.; Govil, H.; Gill, N.; Dey, A. A long-term seasonal analysis on the relationship between LST and NDBI using Landsat data. *Quat. Int.* **2021**, *575*, 249–258. [[CrossRef](#)]
46. Bakillah, M.; Liang, S.; Mobasheri, A.; Jokar Arsanjani, J.; Zipf, A. Fine-resolution population mapping using OpenStreetMap points-of-interest. *Int. J. Geogr. Inf. Sci.* **2014**, *28*, 1940–1963. [[CrossRef](#)]
47. McKenzie, G.; Janowicz, K.; Gao, S.; Gong, L. How where is when? On the regional variability and resolution of geosocial temporal signatures for points of interest. *Comput. Environ. Urban Syst.* **2015**, *54*, 336–346. [[CrossRef](#)]
48. Novack, T.; Peters, R.; Zipf, A. Graph-based matching of points-of-interest from collaborative geo-datasets. *ISPRS Int. J. Geoinf.* **2018**, *7*, 117. [[CrossRef](#)]
49. Wang, J.F.; Li, X.H.; Christakos, G.; Liao, Y.L.; Zhang, T.; Gu, X.; Zheng, X.Y. Geographical detectors-based health risk assessment and its application in the neural tube defects study of the Heshun Region, China. *Int. J. Geogr. Inf. Sci.* **2010**, *24*, 107–127. [[CrossRef](#)]
50. Zhang, L.; Liu, W.; Hou, K.; Lin, J.; Song, C.; Zhou, C.; Huang, B.; Tong, X.; Wang, J.; Rhine, W.; et al. Air pollution exposure associates with increased risk of neonatal jaundice. *Nat. Commun.* **2019**, *10*, 3741. [[CrossRef](#)]
51. Song, Y.; Wang, J.; Ge, Y.; Xu, C. An optimal parameters-based geographical detector model enhances geographic characteristics of explanatory variables for spatial heterogeneity analysis: Cases with different types of spatial data. *Gisci. Remote Sens.* **2020**, *57*, 593–610. [[CrossRef](#)]
52. Luo, W.; Jasiewicz, J.; Stepinski, T.; Wang, J.; Xu, C.; Cang, X. Spatial association between dissection density and environmental factors over the entire conterminous United States. *Geophys. Res. Lett.* **2016**, *43*, 692–700. [[CrossRef](#)]
53. Wang, J.F.; Zhang, T.L.; Fu, B.J. A measure of spatial stratified heterogeneity. *Ecol. Indic.* **2016**, *67*, 250–256. [[CrossRef](#)]
54. He, D.; Zhong, Y.; Zhang, L. Spatiotemporal subpixel geographical evolution mapping. *IEEE Trans. Geosci. Remote* **2018**, *57*, 2198–2220. [[CrossRef](#)]
55. Gibson, J.; Boe-Gibson, G. Nighttime lights and county-level economic activity in the United States: 2001 to 2019. *Remote Sens.* **2021**, *13*, 2741. [[CrossRef](#)]
56. Bluhm, R.; McCord, G.C. What can we learn from nighttime lights for small geographies? measurement errors and heterogeneous elasticities. *Remote Sens.* **2022**, *14*, 1190. [[CrossRef](#)]

57. Huang, Q.; Yang, X.; Gao, B.; Yang, Y.; Zhao, Y. Application of DMSP/OLS nighttime light images: A meta-analysis and a systematic literature review. *Remote Sens.* **2014**, *6*, 6844–6866. [[CrossRef](#)]
58. Ma, J.; Guo, J.; Ahmad, S.; Li, Z.; Hong, J. Constructing a new inter-calibration method for DMSP-OLS and NPP-VIIRS nighttime light. *Remote Sens.* **2020**, *12*, 937. [[CrossRef](#)]
59. Li, X.; Zhan, C.; Tao, J.; Li, L. Long-term monitoring of the impacts of disaster on human activity using DMSP/OLS nighttime light data: A case study of the 2008 Wenchuan, China Earthquake. *Remote Sens.* **2018**, *10*, 588. [[CrossRef](#)]
60. Xia, C.; Yeh AG, O.; Zhang, A. Analyzing spatial relationships between urban land use intensity and urban vitality at street block level: A case study of five Chinese megacities. *Landsc. Urban Plan.* **2020**, *193*, 103669. [[CrossRef](#)]
61. Zhuo, L.; Ichinose, T.; Zheng, J.; Chen, J.; Shi, P.J.; Li, X. Modelling the population density of China at the pixel level based on DMSP/OLS non-radiance-calibrated night-time light images. *Int. J. Remote Sens.* **2009**, *30*, 1003–1018. [[CrossRef](#)]
62. Cao, X.; Wang, J.; Chen, J.; Shi, F. Spatialization of electricity consumption of China using saturation-corrected DMSP-OLS data. *Int. J. Appl. Earth Obs.* **2014**, *28*, 193–200. [[CrossRef](#)]
63. Pan, J.H.; Li, J.F. Estimate and spatio-temporal dynamics of electricity consumption in China based on DMSP/OLS images. *Geogr. Res.* **2016**, *35*, 627–638.
64. He, C.; Ma, Q.; Li, T.; Yang, Y.; Liu, Z. Spatiotemporal dynamics of electric power consumption in Chinese Mainland from 1995 to 2008 modeled using DMSP/OLS stable nighttime lights data. *J. Geogr. Sci.* **2012**, *22*, 125–136. [[CrossRef](#)]
65. Wang, Q.; Yuan, T.; Zheng, X.Q. GDP gross analysis at province-level in China based on night-time lightsatellite imagery. *Urban Dev. Stud.* **2013**, *20*, 44–48.